BFS Simulation and Experimental Analysis of the Effect of Ti Additions on the Structure NiAl

Guillermo Bozzolo
Ohio Aerospace Institute, Cleveland, Ohio

Ronald D. Noebe and John Ferrante
Lewis Research Center, Cleveland, Ohio

Anita Garg
A.Y.T. Corporation, Cleveland, Ohio

Frank S. Honecy
Lewis Research Center, Cleveland, Ohio

Carlos Amador
Universidad Nacional Autónoma de México, Mexico D.F., Mexico

The NASA STI Program Office . . . in Profile

Since its founding, NASA has been dedicated to the advancement of aeronautics and space science. The NASA Scientific and Technical Information (STI) Program Office plays a key part in helping NASA maintain this important role.

The NASA STI Program Office is operated by Langley Research Center, the Lead Center for NASA's scientific and technical information. The NASA STI Program Office provides access to the NASA STI Database, the largest collection of aeronautical and space science STI in the world. The Program Office is also NASA's institutional mechanism for disseminating the results of its research and development activities. These results are published by NASA in the NASA STI Report Series, which includes the following report types:

- TECHNICAL PUBLICATION. Reports of completed research or a major significant phase of research that present the results of NASA programs and include extensive data or theoretical analysis. Includes compilations of significant scientific and technical data and information deemed to be of continuing reference value. NASA's counterpart of peer-reviewed formal professional papers but has less stringent limitations on manuscript length and extent of graphic presentations.

- TECHNICAL MEMORANDUM. Scientific and technical findings that are preliminary or of specialized interest, e.g., quick release reports, working papers, and bibliographies that contain minimal annotation. Does not contain extensive analysis.

- CONTRACTOR REPORT. Scientific and technical findings by NASA-sponsored contractors and grantees.

- CONFERENCE PUBLICATION. Collected papers from scientific and technical conferences, symposia, seminars, or other meetings sponsored or cosponsored by NASA.

- SPECIAL PUBLICATION. Scientific, technical, or historical information from NASA programs, projects, and missions, often concerned with subjects having substantial public interest.

- TECHNICAL TRANSLATION. English-language translations of foreign scientific and technical material pertinent to NASA's mission.

Specialized services that complement the STI Program Office's diverse offerings include creating custom thesauri, building customized data bases, organizing and publishing research results . . . even providing videos.

For more information about the NASA STI Program Office, see the following:

- Access the NASA STI Program Home Page at *http://www.sti.nasa.gov*

- E-mail your question via the Internet to help@sti.nasa.gov

- Fax your question to the NASA Access Help Desk at (301) 621-0134

- Telephone the NASA Access Help Desk at (301) 621-0390

- Write to:
  NASA Access Help Desk
  NASA Center for AeroSpace Information
  7121 Standard Drive
  Hanover, MD 21076

BFS Simulation and Experimental Analysis of the Effect of Ti Additions on the Structure NiAl

Guillermo Bozzolo
Ohio Aerospace Institute, Cleveland, Ohio

Ronald D. Noebe and John Ferrante
Lewis Research Center, Cleveland, Ohio

Anita Garg
A.Y.T. Corporation, Cleveland, Ohio

Frank S. Honecy
Lewis Research Center, Cleveland, Ohio

Carlos Amador
Universidad Nacional Autónoma de México, Mexico D.F., Mexico

National Aeronautics and
Space Administration

Lewis Research Center

January 1999

Acknowledgments

Available from

NASA Center for Aerospace Information
7121 Standard Drive
Hanover, MD 21076
Price Code: A04

National Technical Information Service
5285 Port Royal Road
Springfield, VA 22100
Price Code: A04

BFS SIMULATION AND EXPERIMENTAL ANALYSIS OF THE EFFECT OF Ti ADDITIONS ON THE STRUCTURE OF NiAl

Guillermo Bozzolo[a], Ronald D. Noebe[b], John Ferrante[b], Anita Garg[c], Frank S. Honecy[b] and Carlos Amador[d]

[a]Ohio Aerospace Institute, 22800 Cedar Point Rd., Cleveland, OH 44142, U.S.A.

[b]National Aeronautics and Space Administration, Lewis Research Center, Cleveland, OH 44135, U.S.A.

[c]A.Y.T. Corp., NASA Lewis Research Center, Cleveland, OH 44135, U.S.A.

[d]Facultad de Quimica, Universidad Nacional Autonoma de Mexico, Mexico D.F., Mexico.

SUMMARY

The Bozzolo-Ferrante-Smith (BFS) method for alloy energetics is applied to the study of ternary additions to NiAl. A description of the method and its application to alloy design is given. Two different approaches are used in the analysis of the effect of Ti additions to NiAl. First, a thorough analytical study is performed, where the energy of formation, lattice parameter and bulk modulus are calculated for a large number of possible atomic distributions of Ni, Al and Ti. Substitutional site preference schemes and formation of precipitates are thus predicted and analyzed. The second approach used consists of the determination of temperature effects on the final results, as obtained by performing a number of large scale numerical simulations using the Monte Carlo-Metropolis procedure and BFS for the calculation of the energy at every step in the simulation. The results indicate a sharp preference of Ti for Al sites in Ni-rich NiAl alloys and the formation of ternary Heusler precipitates beyond the predicted solubility limit of 5 at. % Ti. Experimental analysis of three Ni-Al-Ti alloys confirms the theoretical predictions.

KEYWORDS: Alloys, Intermetallics, BFS Method, Defect Structure, Semiempirical Methods, Ternary Alloy, Heusler phase

INTRODUCTION

The development of more efficient gas turbine engines and power plants for future supersonic transports like the high speed civil transport (HSCT) depends upon the advancement of new high-temperature materials with temperature capabilities exceeding those of current nickel-base super-alloys. Ordered intermetallic alloys, in particular the B2 structured NiAl, have long been considered a prime candidate to replace superalloys in the combustion and turbine sections of aircraft engines due to a number of property advantages including the recent development of alloying schemes for enhanced creep strength [1].

One of the most basic of these strategies is to combine single crystal processing and alloying with reactive elements such as Ti, Hf, Zr and Ta in order to generate extremely creep resistant materials [2]. This approach has been so effective that single-crystal NiAl alloy turbine vanes have been successfully engine tested [3]. Not only did the parts survive engine testing but they displayed superior performance to superalloy components undergoing the same evaluation. However, alloy design, while successful to this point, has been entirely empirical in nature. Furthermore, limited understanding of the basic microstructures and structure-property relationships has occurred due to this empirical alloy design approach. For example, Ti additions on the order of 2.5-3.0 at. % result in a 200-5000 fold reduction in creep rate over binary NiAl single crystals and Hf additions can have an even larger effect, but the basic strengthening mechanisms and even the equilibrium microstructures of these materials are unclear [4].

While it is well known that ternary and higher order alloying additions to structural interme-tallics are essential for the optimization of physical, chemical, structural, and mechanical proper-ties, it is only recently that substantial theoretical work has been directed towards a thorough understanding of the atomic processes involved. In the simple cases of FeAl and NiAl, there are

abundant, sometimes conflicting results from a variety of techniques, providing some guidance as to the defect structures in these binary compounds as a function of stoichiometry [1,5-7]. From a theoretical standpoint, first-principles calculations have also provided very valuable information regarding this issue [8]. However, a full understanding of the atomic-level processes involved and a complete description of the composition and temperature dependence of point defects and site substitution schemes for alloying additions are not yet available for NiAl and FeAl. This problem is even more pronounced for alloy systems which have not been as thoroughly studied and is nearly intractable for quaternary and higher order additions to an ordered A-B system.

While it would be extremely advantageous to perform accurate quantitative and qualitative theoretical analysis of these multicomponent systems, this is beyond the scope of most currently available techniques. Theoretical predictions of alloy properties are generally obtained by two approaches, first-principles and semiempirical. First-principles methods involve solving Schroedinger's equation for the system at hand, while semiempirical methods attempt to develop approaches to model energetics with empirical input to obtain unknown parameters. Ideally, first principles calculations are best suited for providing the most accurate and consistent framework for such studies. However, the small differences in energy related to basic issues like preferential site substitution impose the need for intensive electronic structure calculations. Moreover, the complexity of the multi-component systems imposes further limitations, and thus, not enough information can be realistically expected from a first-principles approach because the CPU intensive calculations must be performed for many possible, large configurations. This limits the usefulness of first principles approaches as economical predictive tools.

On the other hand, semiempirical approaches partially solve this problem by introducing a much needed degree of efficiency, which enables one to look at larger systems, at the expense of

a hopefully minimal loss of physical accuracy. Most importantly, they are useful in providing a global view of the mechanisms or processes at hand. However, their range is limited, in most cases, to a few elements or some particular crystallographic structure. Furthermore, methods that exhibit a great deal of accuracy for bulk materials fail to reproduce some of the most basic properties of surfaces or grain boundaries. In addition, their field of applicability to monatomic systems or very specific binary systems (for which specific parameterizations or potentials are often developed) is limited due to the lack of transferrability of the parameters used. Recently, a new semiempirical technique was developed which avoids these current limitations. The BFS (Bozzolo- Ferrante-Smith) method for alloys [10] is particularly designed to deal with complex systems and geometries; it has no constraints regarding the atomic species under consideration, their number, or the crystallographic structure. The BFS method provides a simple framework for large scale computer simulations with the appropriate formal background, but without the limitations that exist in competing techniques.

After a brief introduction of the BFS method, this paper concentrates on its application to the study of ternary Ni-Al-Ti alloys, focusing on physical properties, resulting defect structures, the solubility of Ti in NiAl and precipitation of second phases. A discussion of the lattice parameter dependence with composition based on a simple, approximate expression is also included. Moreover, the results include Monte Carlo temperature-dependent large-scale simulations providing some insight on final equilibrium microstructures. Finally, owing to the engineering significance of NiAl-Ti alloys and to develop confidence in the modeling effort, the theoretical results derived from the BFS method are compared to the results from a concurrent transmission electron microscopy study.

THE BFS METHOD

Since its inception a few years ago, the BFS method [9-11] has been applied to a variety of problems, ranging from bulk properties of solid solutions of fcc and bcc binary alloys [11-12] to more specific applications like the energetics of bimetallic tip-sample interactions in an atomic force microscope [13]. More recently, the BFS method was used to deal with alloy surfaces as well as the phase stability in bulk alloys, which has been illustrated in detailed studies and simulations of surface alloys [14] and the design of Ni-based quaternary alloys [10], providing a foundation for the work presented in this paper. In addition, through BFS we can derive simple, approximate expressions that describe trends in segregation as well as elucidating driving mechanisms for these phenomena [15]. Also, simple expressions can be derived for predicting the composition dependence of bulk alloy properties based solely on pure component properties (the BF rule) [16].

In what follows, we provide a brief description of the operational equations of BFS in order to introduce some concepts used later on. The reader is encouraged to seek further details in previous papers where a detailed presentation of the foundation of the method, its basis in perturbation theory, and a discussion of the approximations made are clearly shown [9,10].

The BFS method provides a simple algorithm for the calculation of the energy of formation of an arbitrary alloy (the difference between the energy of the alloy and that of its individual constituents). In BFS, the energy of formation is written as the superposition of individual contributions of all the atoms in the alloy

$$\Delta H = \sum_i \varepsilon_i \qquad (1)$$

For each atom, we partition the energy into two parts: a strain energy and a chemical energy contribution. The strain energy is based on the atomic positions of the neighboring atoms to atom i, regardless of their chemical identity. For its calculation, we use the actual geometrical distribution of the atoms surrounding atom i, computed as if all of its neighbors were of the same species as atom i. In this sense, the BFS strain energy differs from the commonly defined strain energy in that the actual chemical environment is replaced by that of a monatomic crystal. Its calculation is then straightforward, even amenable to first-principles techniques. In our work, we use Equivalent Crystal Theory (ECT) [17] for its computation, due to its proven ability to provide accurate and computationally economical answers to most general situations. In all cases considered in this work, a rigorous application of ECT is reduced to that of its two leading terms, describing average density contributions and bond-compression anisotropies and neglecting the three- and four-body terms dealing with the bond angle and face-diagonal anisotropies [17].

The chemical environment of atom i is considered in the computation of the BFS chemical energy contribution, where the surrounding atoms are forced to occupy equilibrium lattice sites corresponding to the reference atom i. Building on the concepts of ECT, a straightforward approach for the calculation of the chemical energy is defined, properly parameterizing the interaction between dissimilar atoms.

Thus defined, the BFS strain and chemical energy contributions take into account different effects, i.e. geometry and composition, computing them as isolated effects. A coupling function g restores the relationship between the two terms, defined in such away as to properly consider the asymptotic behavior where chemical effects are negligible for large separations between dissimilar atoms.

Simply, the contribution from each atom i to the energy of formation ΔH is

$$\varepsilon_i = e_S + g\varepsilon_C = e_S + g(e_C - e_{C_0}) \tag{2}$$

where ε_C is the chemical energy of the atom (e_C) referenced to its pure ground state crystal (e_{C_0}).

The strain energy contribution is obtained by solving the ECT perturbation equation

$$NR_1^p e^{-\alpha R_1} + MR_2^p e^{-\left(\alpha + \frac{1}{\lambda}\right)R_2} = \sum_j r_j^p e^{-(\alpha + S(r))r_j} \tag{3}$$

where N and M are the number of nearest- and next-nearest neighbors respectively, and where $p, l,$ α and λ are ECT parameters that describe element i (see Ref. 17 for definitions and details), r denotes the distance between the reference atom and each of its neighbors and $S(r)$ describes a screening function [17] and the sum runs over nearest and next nearest neighbors. This equation determines the lattice parameter a_S of a perfect, equivalent crystal where the reference atom i has the same energy as it has in the geometrical environment of the alloy. R_1 and R_2 denote the nearest- and next-nearest neighbor distances in this equivalent crystal.

Once the lattice parameter of the (strain) equivalent crystal , a_S , is determined, the BFS strain energy contribution is computed using the Universal Binding Energy Relation (UBER) of Rose et al. [18], which contains all the relevant information concerning a single-component system:

$$e_S = E_C\left(1 - (1 + a_S^*)e^{-a_S^*}\right) \tag{4}$$

where E_C is the cohesive energy of atom i and where the scaled lattice parameter a_S^* is given by

$$a_S^* = q\frac{(a_S - a_e)}{l} \tag{5}$$

where q is the ratio between the equilibrium Wigner-Seitz radius and the equilibrium lattice parameter a_e.

The BFS chemical energy is obtained by a similar procedure. As opposed to the strain energy term, the surrounding atoms retain their chemical identity, but are forced to be in equilibrium lattice sites of an equilibrium (otherwise monatomic) crystal i . The BFS equation for the chemical energy is given by

$$NR_1^{p_i}e^{-\alpha_i R_1} + MR_2^{p_i}e^{-\left(\alpha_i + \frac{1}{\lambda_i}\right)R_2} = \sum_k \left(N_{ik}r_1^{p_i}e^{-\alpha_{ik}r_k} + M_{ik}r_2^{p_i}e^{-\left(\alpha_{ik} + \frac{1}{\lambda_i}\right)r_2} \right) \qquad (6)$$

where N_{ik} and M_{ik} are the number of nearest- and next-nearest neighbors of species k to atom i.

The chemical environment surrounding atom i is reflected in the parameters α_{ik}, given by

$$\alpha_{ik} = \alpha_i + \Delta_{ki} \qquad (7)$$

where the BFS parameters Δ_{ki} (a perturbation on the single-element ECT parameter α_i) describe the changes of the wave function in the overlap region between atom i and k. Once Eq. (6) is solved for the equivalent chemical lattice parameter a_C, the BFS chemical energy is then

$$e_C = \gamma_i E_C^i \left(1 - (1 + a_C^*)e^{-a_C^*} \right) \qquad (8)$$

where $\gamma_i = 1$ if $a_C^* > 0$ and $\gamma_i = -1$ if $a_C^* < 0$. The scaled chemical lattice parameter is given by

$$a_C^* = q \frac{(a_C - a_e)}{l_i} \qquad\qquad (9)$$

A reference chemical energy contribution e_{C_o} is also computed, in order to free the BFS chemical energy from any structural information [9,10]. This is accomplished by repeating the process for computing e_C (using Eqs. 6 and 8) but setting the BFS parameters Δ_{ki} to zero. The total BFS chemical energy ε_C (Eq. 2) is then

$$\varepsilon_C = e_C - e_{C_0}. \qquad\qquad (10)$$

Finally, as mentioned above, the BFS chemical and strain contributions are linked by a coupling function g which describes the influence of the geometrical distribution of the surrounding atoms in the relevance of the chemical effects, and is given by

$$g_i = e^{-a_S^*} \qquad\qquad (11)$$

In this work we used the BFS interaction parameters Δ determined following the procedure outlined in Ref. 9. These parameters are obtained from first-principles, all-electron, density functional calculations of the elemental constituents and ordered binary compounds of these elements [19,20]. The particular implementation used is the Linear-Muffin-Tin Orbitals (LMTO) method [10] in the Atomic Sphere Approximation. As mentioned above, in order to provide parameters to the BFS method, we need to calculate the equilibrium properties of the elemental solids in the

same symmetry as the compound to be studied, since BFS is referenced to the ground state properties of the system in that symmetry. Therefore, for this study, Ni, Al and Ti input parameters were calculated for the bcc symmetry (Table 1). Also, BFS interaction parameters Δ_{AB} and Δ_{BA} were determined for Ni-Al, Ni-Ti and Ti-Al in the bcc symmetry by fitting to LMTO-computed

TABLE 1
COMPUTED CONSTANTS AND INPUT FOR ECT

	LMTO results			ECT Parameters			
Atom	Lattice Parameter (Å)	Cohesive Energy (eV/atom)	Bulk Modulus (GPa)	p	α (Å^{-1})	l (Å)	λ (Å)
Ni	2.752	5.869	249.2	6	3.0670	0.763	0.2716
Al	3.192	3.942	77.3	4	1.8756	1.038	0.3695
Ti	3.213	6.270	121.0	6	2.6805	1.048	0.3728

LMTO results for the lattice parameter, cohesive energy and bulk modulus for the bcc phases of Ni, Al and Ti. The last four columns list the ensuing ECT parameters determined from the LMTO results.

TABLE 2
INPUT FOR BFS

BFS Parameters (Å^{-1})		
A-B	Δ_{AB}	Δ_{BA}
Ni-Al	-0.05813	0.0822
Ni-Ti	-0.06587	0.4610
Al-Ti	-0.06360	0.2283

BFS parameters Δ_{AB} and Δ_{BA} for Ni-Al, Ni-Ti and Al-Ti determined by fitting the lattice parameter and energy of formation of the corresponding B2 compounds via LMTO calculations.

energies of formation ΔH and equilibrium lattice parameter a_0 for the corresponding B2 alloys (Table 2).

Once these parameters are computed, they remain the same for any other calculation involving any of these elements, requiring no further adjustment or replacement unless the crystal symmetry we are dealing with changes.

Ni-Al-Ti ALLOYS

From a practical standpoint two-phase alloys based on a NiAl matrix reinforced by Heusler (Ni_2AlTi) precipitates have been receiving increased experimental attention due to their potential as high temperature structural alloys [2-4,25-28]. The Heusler phase has a cubic $L2_1$ structure, in which the unit cell is comprised of eight bcc unit cells with Al and Ti atoms occupying two sets of octahedral sites located at body-center locations (Fig. 1). It is related to the B2-NiAl structure in that every other Al site in the NiAl lattice becomes occupied by a Ti atom in an ordered fashion.
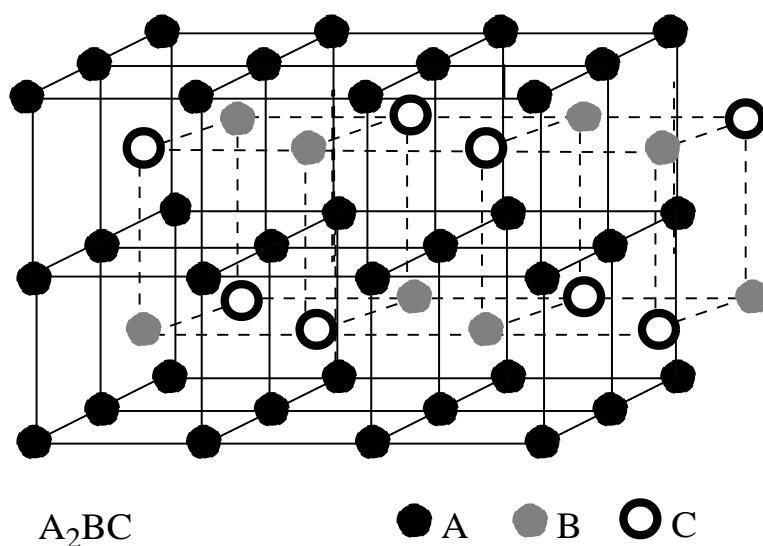

A_2BC •A •B ○C

Fig. 1 : Schematic illustration of the Heusler phase and its relation to B2 compounds.

Because of the similarity in lattice structure between B2 and $L2_1$, it is possible to develop precipitation hardened alloys similar to γ/γ' nickel base superalloys. However, in order to design within this new family of $B2/L2_1$ alloys (also known as β/β' superalloys), microstructural factors such as the solubility of Ti in NiAl, the defect structure within the solid solution NiAl-Ti phase, the lattice misfit between the two phases, and eventually the effect of quaternary and higher order alloying additions on all of these factors need to be determined in detail. However, even with the amount of experimental work performed on the ternary NiAl-Ti system over the last decade [2-4,25-28], details of these microstructural features are still vague while those for quaternary and higher order systems are completely lacking.

Fu et al. [29] have recently presented a comprehensive first principles study of site substitution on both the defect structure of FeAl and NiAl compounds as well as the behavior of ternary (Ti or Cr in FeAl and Fe in NiAl) additions to these systems. Unfortunately, no NiAl+Ti results were included. In a much earlier study, Tso and Sanchez [30] performed some thermodynamic modeling of the Ni-Al-Ti system but the results focused on modeling of the various binary phase diagrams with limited attention and no detail presented concerning the case of ternary alloys.

In this paper, we concentrate on Ni-rich NiAl alloys with Ti alloying additions, prevalent in industrial applications [3,4]. It is essential that the basic properties of the NiAl alloy be accurately reproduced by the use of the BFS method. As seen in Ref. 9, the defect structure of binary NiAl alloys consists primarily of substitutional antisite defects on the Al sublattice and as a result the lattice parameter monotonically decreases with increasing Ni concentration [1]. In a previous application of the BFS method to the study of the zero temperature defect structure of NiAl alloys [9,31], the computational results correctly identified the energetically favored defect structures, including the correct substitutional defect scheme in Ni-rich alloys. It was also shown that while
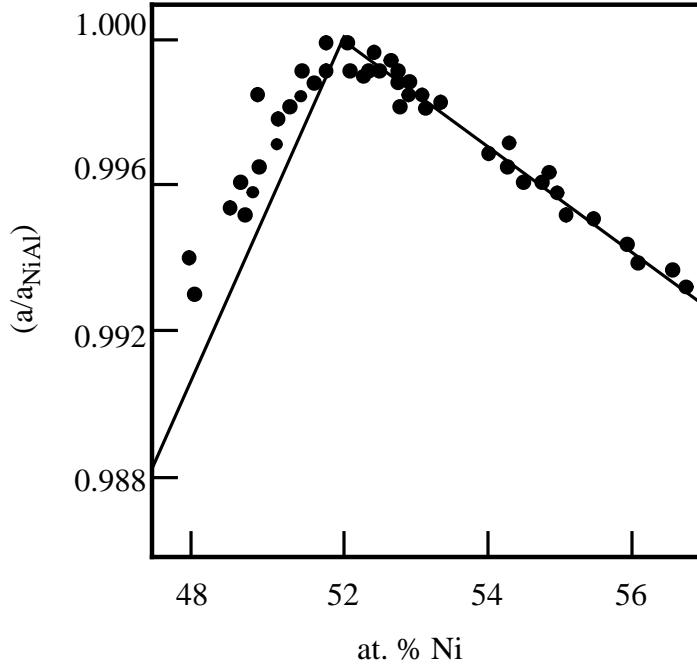
Fig. 2 : Lattice parameter of non-stoichiometric NiAl alloys as a function of Ni concentration, normalized to their stoichiometric values. The solid circles denote experimental results from different investigators (see Ref. 1). The lines denote the BFS predictions.

Ni vacancies are mostly responsible for the observed behavior in Al-rich alloys, evidence was found for the possibility of vacant sites in both sublattices as well as a trend for clustering of vacancies. Both features have been observed in recent experiments [32].

In particular, the quantitative accuracy of the BFS results for binary NiAl is highlighted by the predicted values of the lattice parameter. A survey of available experimental data indicates that the lattice parameter in the Ni-rich region varies linearly with concentration [1]. Correspondingly, the BFS results can be adjusted to a similar linear regime with a very small departure from the experimental expressions:

$$\left(\frac{a}{a_0}\right)_{Exp} = 1.0384 - 0.0007914 x_{Ni} \tag{12}$$

and

$$\left(\frac{a}{a_0}\right)_{BFS} = 1.0396 - 0.0007689 x_{Ni} \qquad (13)$$

where x_{Ni} denotes the atomic concentration of Ni. Fig. 2 displays both the experimental values as well as the two linear regions representing the theoretical results. The qualitative and quantitative agreement with experiment certify the validity of the Ni-Ni, Al-Al and Ni-Al BFS parameters used in this work (listed in Table 2). From a methodological point of view, the good agreement between theoretical and experimental results that follow can be taken as evidence for the validity of the BFS parameters used in this paper.

Analytical Structures

By exploiting the computational simplicity of semiempirical methods and in particular the BFS method, it is possible to analize the energetics of a large number of Ni-Al-Ti alloys. These alloys represent a wide range of concentrations and different atomic distributions with different degrees and types of ordering. For reasons of simplicity and to enable comparison with available experimental data on industrially relevant compositions, we restrict our calculations to Ni-rich $Ni_{50}Al_{50-x}Ti_x$ alloys. The large size of the necessary computational cells combined with the number of different elements considered results in a large number of possible distributions of these atoms within the computational cell chosen. Consequently, an efficient and economical - but physically sound - technique is required to examine all pertinent configurations of atoms. While a search of every possible atomic arrangement in a reasonably large computational cell is not

impossible, we seek to develop a simplified approach that would not only make it more physically intuitive, but also amenable to extensions to larger systems without fearing reaching the limit of the available computational tools.

In this section, we use a similar approach to that used in Ref. 9, representing a compromise between a detailed analytical study and an exhaustive statistical survey for each concentration and atomic distribution. The procedure followed in Ref. 9 consisted of definining a specific set of atomic `configurations', and then using the BFS method to compute the energy of formation of each configuration, as well as its equilibrium lattice parameter and bulk modulus. A large set of high symmetry configurations covering a wide composition range was defined in this manner. The contents of this catalogue of configurations is, to great extent, arbitrary. However, a ternary system is still simple enough to develop an intuitive algorithm for constructing configurations of potential interest. A similar approach is used in this work to examine ternary alloys, building on the originally defined set of configurations including some selected arrangements of atoms that represent different ordering patterns. The purpose of this approach is to 1) relate general trends of the lattice parameter and the energy of formation to changes in concentration and atomic distribution and 2) identify metastable structures, that is, configurations with energy close to that of the ground state, which might have a high probability of appearing in the actual alloy depending on the conditions prevalent during its processing. Therefore, this `catalogue' of alternative configurations serves the purpose of identifying ordering trends and provides physical insight to the microstructure of the actual alloy. Since the number of possible configurations could become prohibitively large, we believe that this selection procedure, when properly undertaken, is sufficient to gain an adequate understanding of the alloy composition under investigation. Some selected configurations are described in Fig. 3. The labeled 72-atom computational cell is shown

(a)

(b)

$[Al \longrightarrow Ti]_{37\text{-}48} + Ni_{49\text{-}60} \longleftrightarrow Al_{61\text{-}72}$

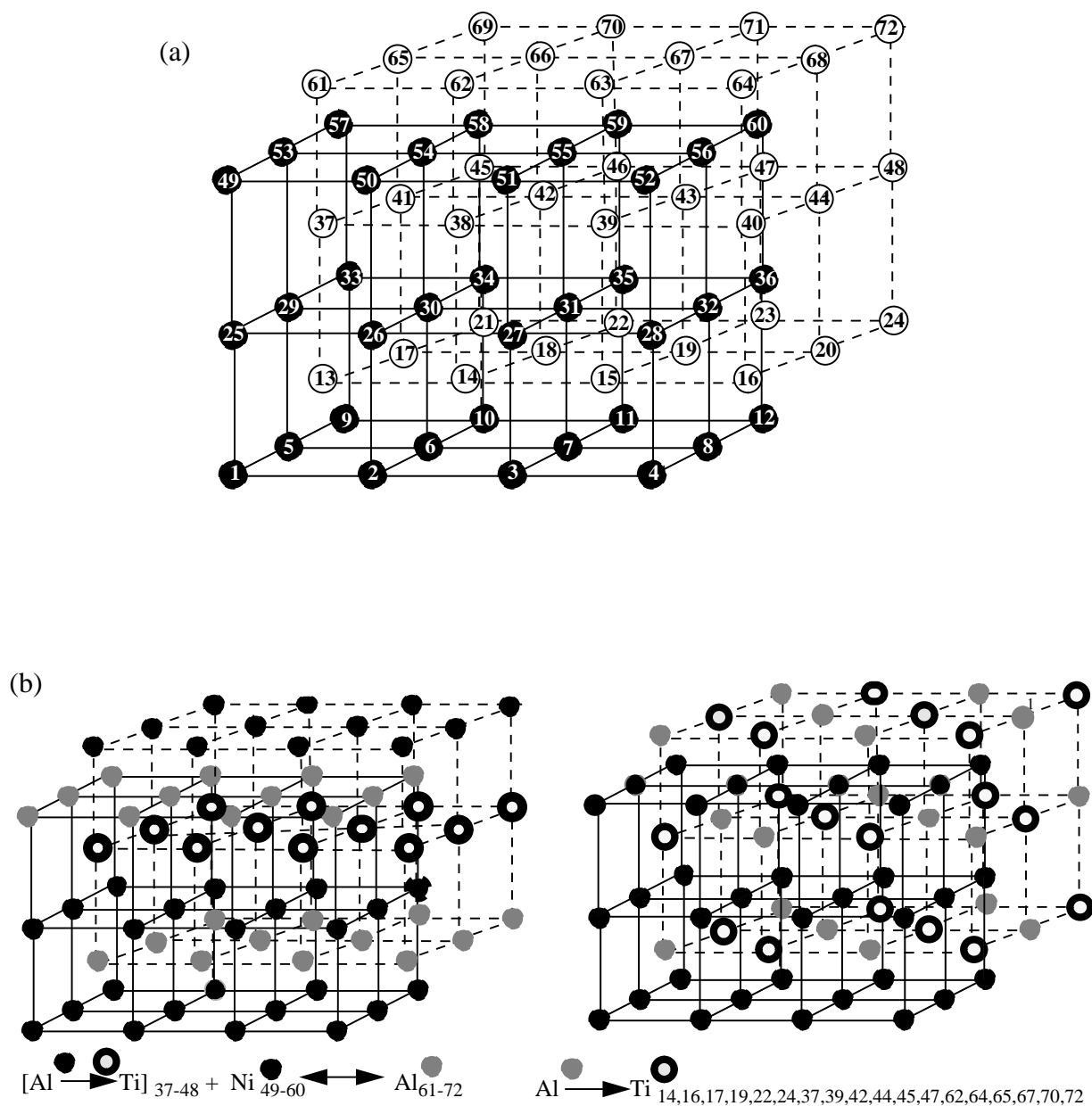$Al \longrightarrow Ti_{14,16,17,19,22,24,37,39,42,44,45,47,62,64,65,67,70,72}$

Fig. 3 (a) The computational cell used to generate the catalogue shown in the Appendix. (b-c) Two examples of the configurations of NiAl-Ti alloys used in this calculation, corresponding to (b) $x_{Ti} = 13.89$ and (c) $x_{Ti} = 25.00$. In these last two cases, the label indicates the type of substitution. $X_n \to Y_m$ indicates an atom of species X, originally in site n, substituting for an atom of species Y in site m.

in Fig. 3.a to clarify the atomic exchanges that define the different configurations in the set. Two examples of such configurations are shown in Fig. 3.b and 3.c, and a complete list of the configurations studied in this work is included in the Appendix.

The obvious difficulty in defining an appropriate set of configurations for the study at hand is the lack of a priori knowledge of the ground state structure for a given composition or temperature. In some cases (i.e. low concentration solutes) the ground state might have easily predictable features but, in general, no guarantee exists that the ground state configurations for each concentration are included. However, a close examination of the results usually give a clear indication whether a particular configuration could be `missing' from the set if, for example, there are data points 'missing' in what would otherwise be an easily recognizable trend.

In this work, the results for a set of over 150 different configurations or arrangements of a 72-atom computational cell are shown and discussed. Fig. 3 shows two of these configurations and introduces the notation used in the Appendix to identify the positions of Ni, Al and Ti atoms in the lattice. Obviously, if this set was complete and if it included the ground state for a certain composition, the energy of formation for such a configuration would be lower than any other with the same concentration of elements. Moreover, if the catalogue includes the ground state configurations for all concentrations, it would be easy to determine the symmetries that characterize such a state.

Fig. 4 summarizes the results of this type of analysis for the 150+ set of configurations: the energy of formation at zero temperature for $Ni_{50}Al_{50-x}Ti_x$ alloys, for x between 0 (B2 NiAl) and 50 at. % Ti (B2 NiTi), is shown. A close examination of the atomic distributions considered for each concentration -detailed in the Appendix- reveals that most of the likely ordering patterns for a given composition are included in this survey. Moreover, Fig. 4 shows, for each concentration,

`clusters' of states very close in energy that correspond, in terms of the atomic distributions, to related ordering patterns. This behavior is clear throughout the whole range of compositions included, where both end points (NiAl and NiTi) form B2 compounds.

If we focus on those configurations with $0 < x_{Ti} < 25$ %, it is clear that a specific group of configurations, corresponding to the lowest energy states for each concentration above $x_{Ti} = 5$%, fol-
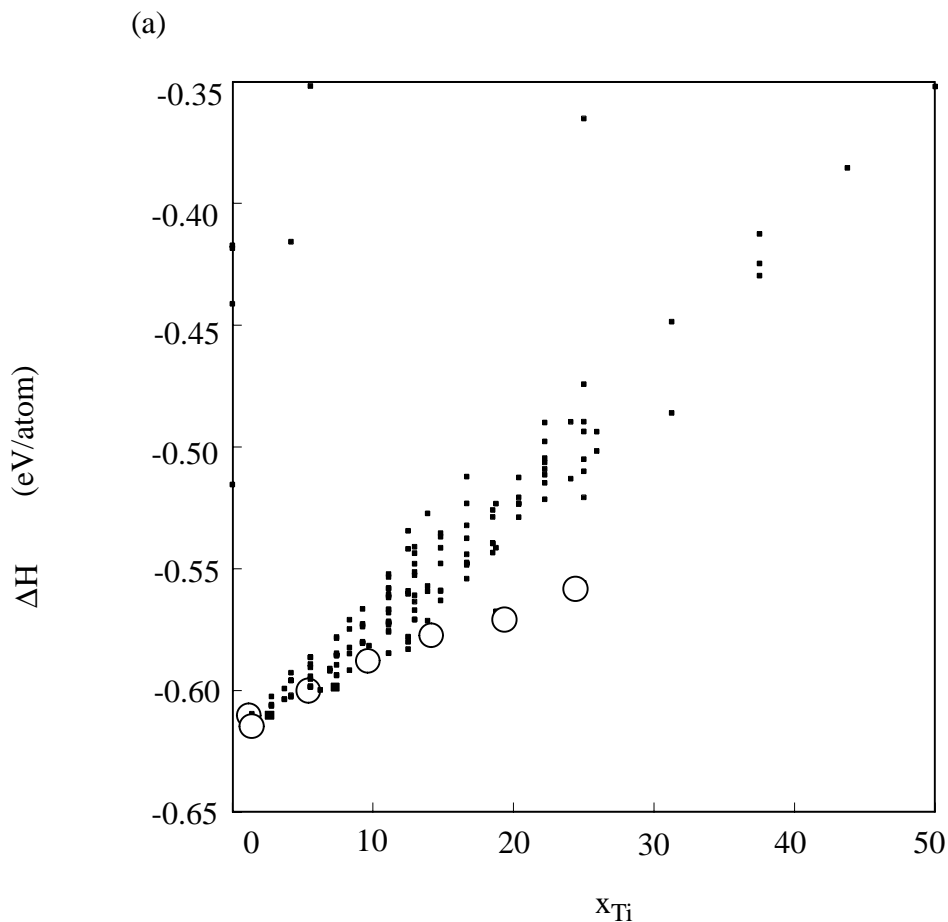
(a)

Fig. 4. Energy of formation (in eV/atom) of the cells listed in the Appendix for $0 < x_{Ti} < 50$. The circles denote those configurations characterized by Heusler ordering, while the solid squares include a variety of short-range order patterns as well as disordered states.

lows a specific ordering trend. We will return to this issue later, once some basic features regarding site preference schemes for the alloying addition are determined.

Site preference of Ti in NiAl alloys

In general, the results in Fig. 4 indicate that those configurations where Ti atoms occupy sites on the Al sublattice are consistently lower in energy. The site preference of Ti atoms can be ana-

TABLE 3
SITE PREFERENCE IN A $Ni_{50}Al_{50-x}Ti_x$ ALLOY

x_{Ti} at. %Ti	Description of the configuration	Energy of Formation (eV)	Lattice Parameter (Å)
1.39	$Ti(Ni)Al_{NN}$	-0.41320	2.870
	$Ti(Ni)Al_{far}$	-0.38052	2.870
	$Ti(Al)$	-0.60839	2.853
2.78	$2Ti(Ni)NN+2Ni(Al)_{NN}$	-0.32607	2.881
	$2[Ti(Ni)Al]_{NN}$	-0.32873	2.882
	$Ti(Ni)Al_{NN}+Ti(Al)$	-0.36893	2.879
	$[Ti(Ni)Al+Ti(Al)]_{far(2a)}$	-0.37773	2.878
	$2Ti(Al)_{NN}$	-0.59918	2.859
	$2Ti(Al)_{far(\sqrt{2}a)}$	-0.60350	2.858
	$2Ti(Al)_{Heusler}$	-0.60350	2.858
	$2Ti(Al)_{far(\sqrt{3}a)}$	-0.60363	2.858

Energy of formation (in eV/atom) and lattice parameter (in Å) for specific atomic configurations of Ti atoms within a NiAl lattice at two different concentration levels.

lytically determined with the BFS method by considering just a few selected configurations where, for a fixed concentration, Ti atoms are located in specific sites. Figure 5 shows the configurations considered in such a search and Table 3 lists the corresponding values for the energy of formation and equilibrium lattice parameter.

The notation used to indicate site preference is self-explanatory and is convenient for representing more complicated situations as will be seen in subsequent studies dealing with 4- and 5-element systems. The notation A(B) indicates a substitutional defect where atom A occupies a B site. The designation A(B)C indicates an A atom occupying a B site with the displaced B atom occupying a C site. When necessary, the physical separation between two point defects is noted : for example, $A(B)C_{NN}$ indicates that the A atom in the B site and the B atom in the C site are nearest neighbors. In Table 3, the subindex *far(d)* denotes that the corresponding atoms are at a distance *d* greater than second neighbor distances, while the subindex *Heusler* indicates that the atoms locate themselves in Al sites following the Heusler structure (atoms in any pair of Heusler sites are located in opposite corners of a face of the elementary cube in the Al sublattice).

The cases considered for the study of site substitution for low Ti concentration include two different values: 1.39 and 2.78 at. % Ti. For the first case, which represents one Ti atom in the 72-atom cell, two basic configurations are possible: the Ti atom occupying an Al site (Ti(Al)) (fig. 5.a), and the Ti atom occupying a Ni site with the displaced Ni atom located in an Al site (Ti(Ni)Al). In this second type of configuration, the antistructure Ni atom can be a nearest neighbor of the Ti atom ($Ti(Ni)Al_{NN}$, fig. 5.b) or not ($Ti(Ni)Al_{far}$, fig. 5.c). The corresponding values for the energy of formation are listed in Table 3, clearly showing the preference of a Ti atom for an Al site. A similar situation is observed at a higher Ti concentration (figs. 5.d-5.h), which corresponds to two Ti atoms in the 72-atom cell. Several possibilities now exist concerning the relative

(a) Ti(Al)

(b) Ti(Ni)Al$_{NN}$

(c) Ti(Ni)Al$_{far}$

(d) 2Ti(Ni)Al$_{NN}$

(e) Ti(Ni)Al$_{NN}$+Ti(Al)

(f) [Ti(Ni)Al +Ti(Al)]$_{far}$

(g) 2Ti(Al)$_{far}$

(h) 2Ti(Al)$_{Heusler}$
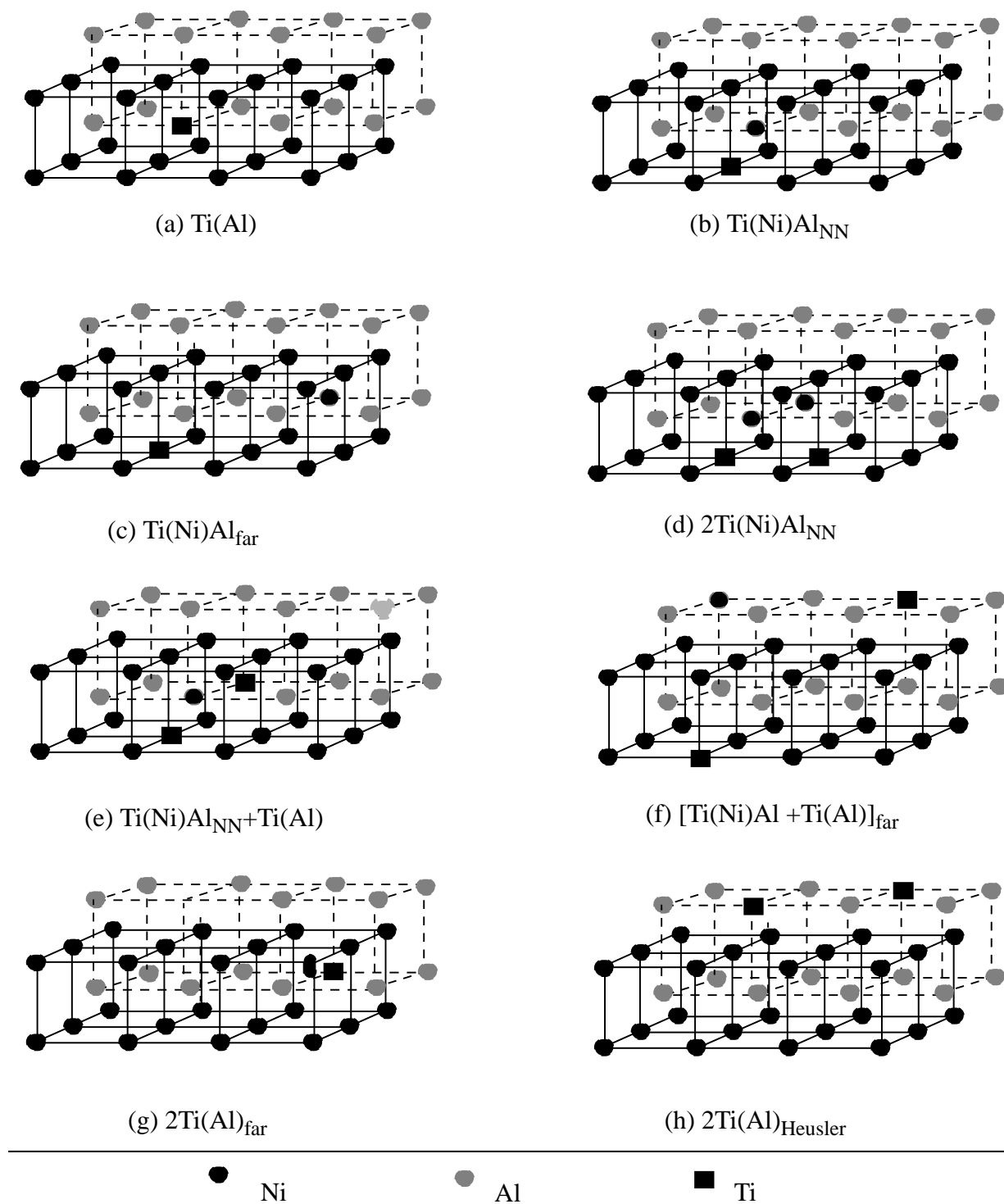
● Ni   ● Al   ■ Ti

Fig. 5 Configurations used for the calculation of Ti site preference in NiAl alloys. (a) A Ti atom in an Al site, (b) a Ti atom in a Ni site, with the displaced Ni atom occupying a site in the Al sublattice at nearest-neighbor distance from the Ti atom, (c) same as before but with the Ni atom located at a different site in the lattice, at a distance greater than next-nearest-neighbor distance, etc.. In all cases, A(B) indicates an atom A in a B site while A(B)C indicates an atom A in a B site with the displaced B atom in a C site.

location of the additional Ti atoms: they could both be located in Al sites (2Ti(Al)), or create an antistructure Ni pair by occupying Ni sites with the Ni atoms occupying Al sites (2Ti(Ni)Al), or a combination of these defects with several options for the relative location of the antistructure and substitutional atoms with regard to each other ([Ti(Al) + Ti(Ni)Al]$_d$).

All these possibilities are included in Fig. 5 and the corresponding formation energies are listed in Table 3. Once again there is a clear preference for Ti to occupy Al sites compared to any other substitution scheme. Moreover, the small difference in energy of formation between the case when the two Ti atoms are nearest neighbors and the case where they are truly separated can be taken as the reason why at low Ti concentrations there is a close competition between a solid solution alloy and an ordered arrangement of Ti atoms on the Al-sublattice, leading to the formation of a precipitate phase, as seen in Fig. 4.b (cases involving ordering of the Ti atoms are indicated with circles while more random configurations of the Ti atoms are indicated with solid squares). The preference of Ti for Al sites is observed for the whole range of Ti concentrations considered in this work, leading eventually to the formation of the Heusler (Ni$_2$AlTi) alloy, where Ti atoms would be exclusively located in the Al sublattice of a B2 compound, leading to the L2$_1$ structure.

Figure 6 is an alternative way of displaying the results of the site preference calculations, in the form of an energy spectrum. The advantages of visualizing the results in this way will become apparent when dealing with 4- and 5-element alloys, clearly indicating the interaction between the different alloying additions. The first column shows the energy `levels' corresponding to the different substitution schemes for just one Ti atom in a 72 atom cell. The second and third columns show results for two (x_{Ti} =2.78) and five (x_{Ti}=6.94) atoms respectively. The splitting of the Ti(Al) level for x_{Ti}=2.78 is due to the different relative locations of the two Ti atoms: they could be non-interacting (`*far*'), situated in a Heusler-like pattern (opposite corners of a cube in the Al sublat-
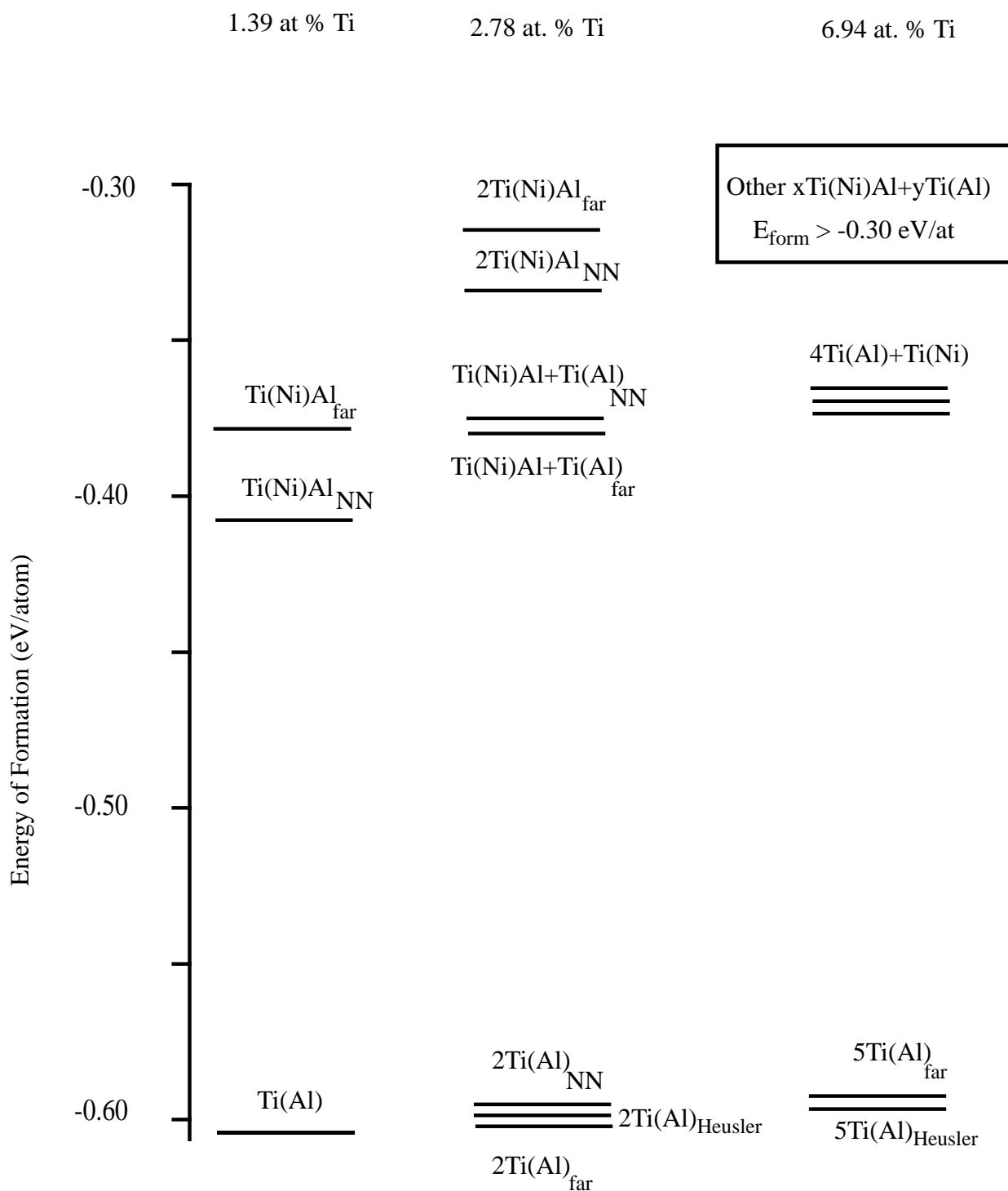
1.39 at % Ti   2.78 at. % Ti   6.94 at. % Ti

$2Ti(Ni)Al_{far}$

$2Ti(Ni)Al_{NN}$

Other $xTi(Ni)Al+yTi(Al)$

$E_{form} > -0.30$ eV/at

$Ti(Ni)Al_{far}$

$Ti(Ni)Al+Ti(Al)_{NN}$

$4Ti(Al)+Ti(Ni)$

$Ti(Ni)Al_{NN}$

$Ti(Ni)Al+Ti(Al)_{far}$

Energy of Formation (eV/atom)

-0.30

-0.40

-0.50

-0.60

$2Ti(Al)_{NN}$

$2Ti(Al)_{Heusler}$

$5Ti(Al)_{far}$

$5Ti(Al)_{Heusler}$

Ti(Al)

$2Ti(Al)_{far}$

Fig. 6: Energies of formation (in eV/atom) for 72 atom cells containing 36 Ni atoms, 36-n Al atoms and n Ti atoms (n = 1, 2, 5). The different energy states correspond to different substitutional and defect schemes, as indicated in Fig. 5.

tice, indicated with circles in Fig. 4.b) or in such a way that the two Ti atoms in the Al sublattice are at next-nearest-neighbor distance from each other. The energy difference between these two states is extremely small at this concentration but it still favors a random distribution of Ti atoms in the Al sublattice. For $x_{Ti} = 6.94$ the splitting in energy levels is much more pronounced since many more possibilities exist for the placement of the Ti atoms. For clarity, we only show two states in the ground state region: the one corresponding to the Ti atoms in solid solution (`far' from each other in the Al sublattice) and the Ti atoms following a strict Heusler ordering pattern. The reversal in energy levels between $x_{Ti} = 2.78$ and $x_{Ti} = 6.94$ for the solid solution and the Heusler ordering options clearly indicates that the formation of Heusler precipitates is favored at higher Ti concentrations. Finally, the stability of the Heusler phase (Fig. 4), where Ti atoms are located exclusively in Al sites, indicates that the site preference observed at low concentrations is the same for the whole range of concentrations for which this phase exists, consistent with the fact that the energy gap between Ti(Al) and Ti(Ni)Al substitutions remains basically unchanged with increasing Ti concentration.

Evolution of second-phase structures within NiAl-Ti alloys

Figure 3 introduces some selected configurations from the complete set used in this work, as well as the notation used in labeling them. A complete list of configurations is included in the Appendix and the energy of formation computed via BFS for all the configurations is shown in Fig. 4. As mentioned before, one feature in Fig. 4 becomes immediately apparent: beyond 5 at. % Ti, there is a clear separation in formation energy between a selected type of configurations (denoted with circles in Fig. 4) and the rest (denoted with solid squares). The selected group of

configurations correspond to a particular type of ordering, where Ti atoms locate themselves exclusively in Al sites in such a way that they always have Al atoms as next nearest neighbors. This ordering pattern, when extended to the case when the concentration of Ti is 25 %, corresponds to the $L2_1$ ordered structure or Heusler phase. At that particular concentration, the energy gap between the Heusler structure (solid circle in Fig. 4.b) and any other configuration is the largest, clearly indicating the stability of the $L2_1$ phase at a stoichiometry equivalent to Ni_2AlTi.

Below 5 at.% Ti, those configurations representing Ti in solid solution within the matrix are energetically favored, however so slightly, over those where short range order dominates. This is more clearly demonstrated in Figure 6. This situation is reversed at a composition near 5 at. % Ti, with an ever more distinguishable preference for Heusler ordering against any other option with increasing Ti content. In other words, Heusler-like ordering becomes clearly preferred beyond a certain critical value somewhere near 5 at. % Ti, in spite of the fact that even at lower concentrations those configurations with short-range Heusler-type ordering are also very low in energy. This crude way of determining the solubility limit of Ti in NiAl, which based on these results could be set somewhere near 5 at. % Ti, not only establishes such a critical value but it also provides some insight on the behavior of the system for a wide range of concentrations surrounding the solubility limit.

One clear reason for the stability of the Heusler phase is the type of nearest neighbor bonds present. The Heusler ordering maximizes the number of energetically favorable Ni-Al and Ni-Ti bonds - both B2 compounds - as seen in Table 4. In addition, the second neighbor bonds are either Ti-Al, also energetically favorable, or Ni-Ni. The Ni-Ni bonds, due to the closeness between the lattice parameter of the Heusler phase to the equilibrium value of the lattice parameter of Ni in its bcc phase, introduce very little strain in the lattice.

TABLE 4: COORDINATION MATRICES FOR Ni, Al AND Ti ATOMS IN TERNARY PHASES

| | Heusler phase | | | | | | Other Ni$_2$AlTi phase | | | | | |
| | Nearest neighbors | | | Next nearest neighbors | | | Nearest neighbors | | | Next nearest neighbors | | |
Atom	Ni	Al	Ti	Ni	Al	Ti	Ni	Al	Ti	Ni	Al	Ti
Ni	0	4	4	6	0	0	0	4	4	6	0	0
Al	8	0	0	0	0	6	8	0	0	0	2	4
Ti	8	0	0	0	6	0	8	0	0	0	4	2

Coordination of nearest-neighbor and next-nearest-neighbor bonds for Ni, Al and Ti atoms in (a) the Heusler phase and (b) the alternate ordering pattern.

A closer examination of the configurations in the Appendix shows that the preference for L2$_1$ ordering is also apparent in the low energy states in the nonselected configurations in Fig. 4. This is because any configuration that contains Ti atoms in Al sites with only Al next nearest neighbors introduces a significant change in energy.

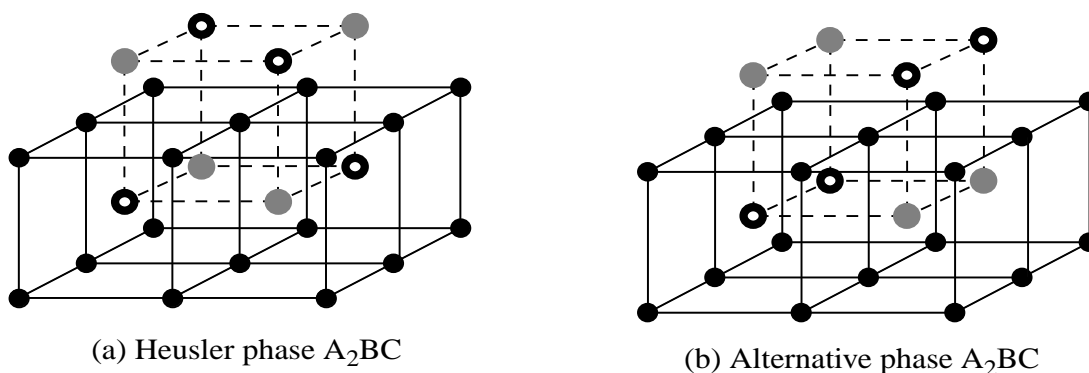(a) Heusler phase A$_2$BC   (b) Alternative phase A$_2$BC

Fig. 7: Schematic representation of (a) Heusler and (b) alternative ternary phases.

An additional advantage of this type of analysis is that a good deal of information on alternative structures can also be obtained. This is an important issue when dealing with metastable structures that may result from a particular processing scheme. For instance, we could examine the energetics of an alternative type of ordering, which for example could involve a slight change in site occupancy in the Al-sublattice. Fig. 7 shows the Heusler unit cell as well as one corresponding to this alternative ordering scheme, which shares the first neighbor coordination with the Heusler phase. The only difference between these structures resides in the second neighbor coordination, with two Ti-Al bonds being replaced by pure Ti-Ti and Al-Al bonds, due to the different distribution of Ti and Al atoms in the Al-sublattice. The equilibrium energy for each of the two cells is, within the precision of these calculations, identical. Therefore, the BFS strain energy contribution for each atom of a given species, in each cell, is the same. Moreover, within the BFS scheme, the only difference in energy between the two structures is due to the different type of next-nearest-neighbors bonds. The creation of Ti-Ti and Al-Al next-nearest neighbor bonds, produces changes in chemical energy resulting in a noticeable change in total energy of formation

TABLE 5
BFS ENERGY CONTRIBUTIONS FOR ORDERED TERNARY PHASES

Atom	Heusler phase			Alternative phase		
	Strain energy (eV/atom)	Chemical energy (eV/atom)	Total BFS energy e (eV/atom)	Strain energy (eV/atom)	Chemical energy (eV/atom)	Total BFS energy e (eV/atom)
Ni	0.108	2.236	1.929	0.108	2.236	1.929
Al	0.503	-1.128	-1.240	0.503	-1.374	-1.622
Ti	0.905	-3.591	-4.782	0.905	-2.680	-3.338

BFS strain (first column), chemical (second column) and total (third column) contributions for each of the two ordered structures shown in Fig. 7.

which favors the location of Ti and Al atoms in the Heusler ordering scheme. Table 5 shows numerical results for the BFS strain, chemical and total energy terms for each type of atom in each type of structure. The total energy of formation for each of the two ordered structures is obtained by $e = (2e_{Ni} + e_{Al} + e_{Ti})/4$, where e_X denotes the BFS energy contribution of an atom of species X. Consequently, the formation energy for the Heusler cell is -0.541 eV/atom whereas the alternating ordering scheme has a higher energy of -0.280 eV/atom.

We then conclude that the changes introduced in chemical energy due to the creation of Ti-Ti and Al-Al next-nearest-neighbors bond makes this configuration energetically less favorable and therefore less likely to be found. However, depending on the processing conditions, it might not be improbable to find short range order similar to that of this alternate ordering scheme (Fig. 7.b) in addition to the expected Heusler ordering in rapidly solidified or quenched alloys. Moreover, in regions with low Ti concentrations, this phase competes with the Heusler phase in that they both share a great deal of common short-range order.

The large difference in energy that can arise between various configurations with the same concentration is not reflected in the corresponding values of the lattice parameters (see Appendix). The lattice parameters of the different ternary alloys considered follow a nearly linear relationship between the binary NiAl and NiTi B2 values as a function of Ti concentration (Fig. 8.a). There is, however, a small deviation above the ideal linear relationship, common to most of the configurations that display short- and long-range order. The overall trend, however, is clear. The lattice parameter of ternary $Ni_{50}Al_{50-x}Ti_x$ alloys increases with increasing Ti content, as confirmed experimentally in Ref. 4. A more detailed display of these results is seen in Fig. 8.b, for Ti concentrations between 0 and 25 at. % Ti.

Table 6 lists the BFS predictions for the lattice parameter of the lowest energy configurations for each concentration. Two sets of values are shown: `*Heusler ordering*', indicating the configuration where Ti atoms locate themselves exclusively in Al sites (with only Al next-nearest-neighbors) following Heusler ordering, and `*Solid Solution*', where the Ti atoms are randomly situated in the Al sublattice. Note that there is no significant difference in lattice parameter for these two configurations.

The results of the first column in Table 6 (`*Ordered*') can be easily adjusted to an expression of the form

$$\frac{a}{a_{NiAl}} = 1.00000 + 0.09347 x_{Ti} \qquad (14)$$

TABLE 6 LATTICE PARAMETER OF
Ni(Al,Ti) ALLOYS

x_{Ti}	Heusler ordering	Solid Solution
2.78	2.856	2.856
4.17	2.859	2.859
5.55	2.863	2.863
6.94	2.867	2.867
8.33	2.871	2.870
9.72	2.875	2.874
11.11	2.879	2.877

Lattice parameter (in Å) of the lowest energy NiAl-Ti configuration for several Ti concentrations (see Appendix for the lattice parameter values for the complete set of configurations used in this work).

plotted in Fig. 8.b, indicating the linear dependence of the lattice parameter of NiAl-Ti alloys with increasing Ti concentration, where a_{NiAl} denotes the equilibrium value of the lattice parameter for stoichiometric NiAl alloys.

The value of these results from this type of analysis is dependent on our ability to build a sufficiently complete catalogue of configurations that includes all the relevant atomic distributions. While the fit includes the lowest energy states that are part of the catalogue, no guarantee exists that these are actually the absolute lowest energy states for this system.

The predicted values for the lattice parameter of NiAl-Ti alloys compare very well with experimental results by Kitabjian et al. [33]. In a recent study of atomic size effects of Ti in NiAl, they calculated the atomic size mismatch $\Delta\Omega_{Ti}$ for Ti atoms replacing Al atoms on the Al sublattice

$$\Delta\Omega_{Ti} = \frac{\Omega^*_{Ti} - \Omega_{Al}}{\Omega_{Al}} \qquad (15)$$

where Ω^*_{Ti} and Ω_{Al} are the atomic volumes of Al and Ti in NiAl. Using their calculated value $\Omega_{Al}=$ 0.134 nm^3, they obtain an approximate expression for $\Delta\Omega_{Ti}$,

$$\Delta\Omega_{Ti} = \frac{3a_0^2}{2\Omega_{Al}}\frac{da}{dx_{Ti}} \qquad (16)$$

where a_0 is the reference lattice parameter of NiAl at $x_{Ni}=0.5$ and da/dx_{Ti} denotes the variation of the lattice parameter of NiAl-Ti alloys with Ti concentration. From measured values for a Ni-47.5Al-2.5Ti alloy, da/dx_{Ti} is estimated to be 0.0364 nm, so that the experimentally determined

value of $\Delta\Omega_{Ti}$ is 0.34, that is, the Ti atom is calculated to be 34 % larger than the Al atom it replaces.

The values of the lattice parameter as a function of Ti concentration predicted with BFS yield $\Delta\Omega_{Ti} = 0.27$, also indicating a large size effect comparable with the experimental value. Considering the constraints imposed in the theoretical calculations, where the physical properties of each element are computed from first-principles calculations [9], as well as the fact that the experimental prediction is based on only one data point, the agreement between experiment and theory seems satisfactory.

The BFS results are also in good agreement with the measured lattice parameters of NiAl-Ti alloys, including the Heusler alloy Ni_2AlTi, reported by Oh-ishi et al. [34]. Using their experimental values for NiAl-Ti and some alloys above the Heusler phase boundary (located at about 20 at. % Ti), Kitabjian et al. [33] computed a size factor of 0.24 for Ti in NiAl, very similar to the value of 0.25 obtained from the corresponding BFS theoretical predictions (using Heusler phase values).

The excellent agreement obtained by including Heusler phase values for the determination of size factors of alloying additions, encourages the use of this approach for those cases where the alloying addition has a very low solubility in the base alloy (i.e., Hf or Zr in NiAl) [33].

The BF Rule

We can validate the theoretical value of these results in a general way by comparing them with alternative approximate algorithms for determining the lattice parameter. The lowest order approximation consists of using Vegard's law [35], which establishes a direct linear average of the

lattice parameter of the constituents. However, this law is rarely valid even for the case of binary systems. Subsequent improvements on Vegard's law highlight the role of compressibility in determining intermediate values of the lattice parameter, in most cases introduced in an *ad hoc* fashion. Recently, a set of approximate expressions based on the BFS method was derived for predicting the lattice parameter of multicomponent systems which naturally introduces the compressibility of the constituents in its formulation. This expression, known as the BF rule has been proven in previous applications to multi-component systems [16], and provides an accurate estimate of the lattice parameter.

The BF rule states that the lattice parameter of a multicomponent system (for elements of the same crystallographic species) is given by

$$a(x_1, x_2, \ldots) = \frac{\sum_{i=1}^{N} a_i^2 B_i}{\sum_{i=1}^{N} a_i B_i} \tag{17}$$

where a_i and B_i are the equilibrium lattice parameter and bulk modulus, respectively, for the *i*th atomic species. Using the parameters listed in Table 1 yields the following expression for NiAl-Ti alloys:

$$a(x_{Ni}, x_{Al}, x_{Ti}) = \frac{1997.32 x_{Ni} + 794.43 x_{Al} + 1249.44 x_{Ti}}{685.80 x_{Ni} + 248.88 x_{Al} + 388.87 x_{Ti}} \tag{18}$$
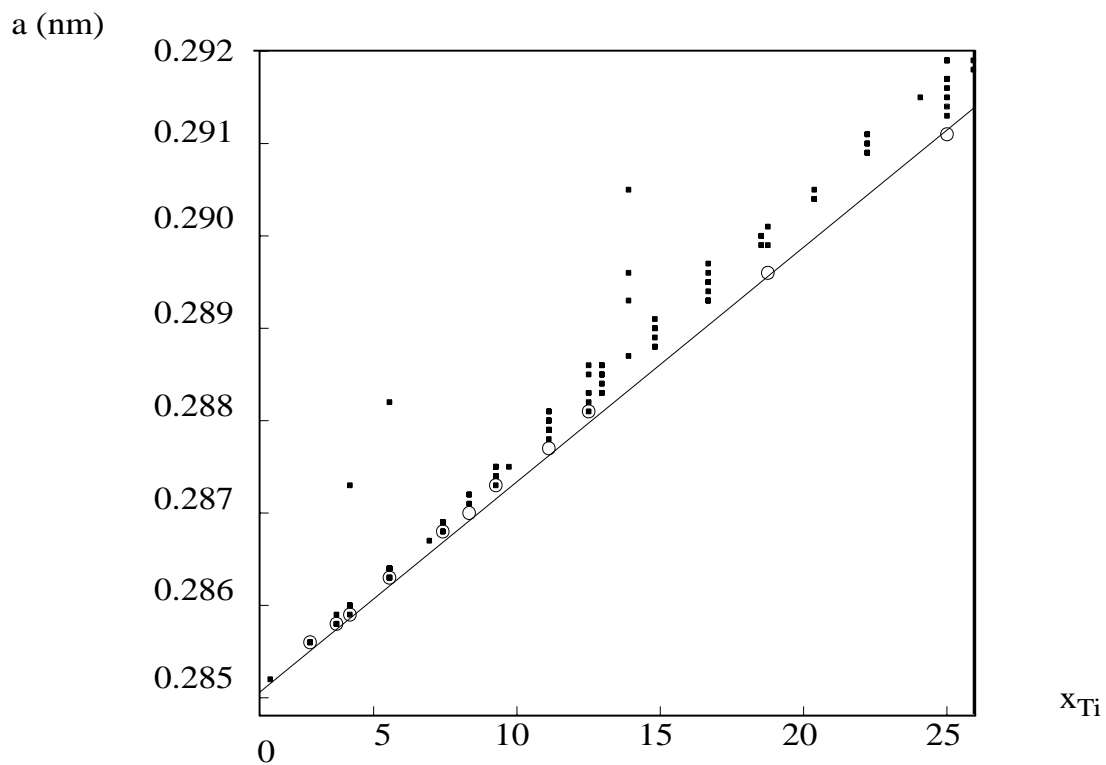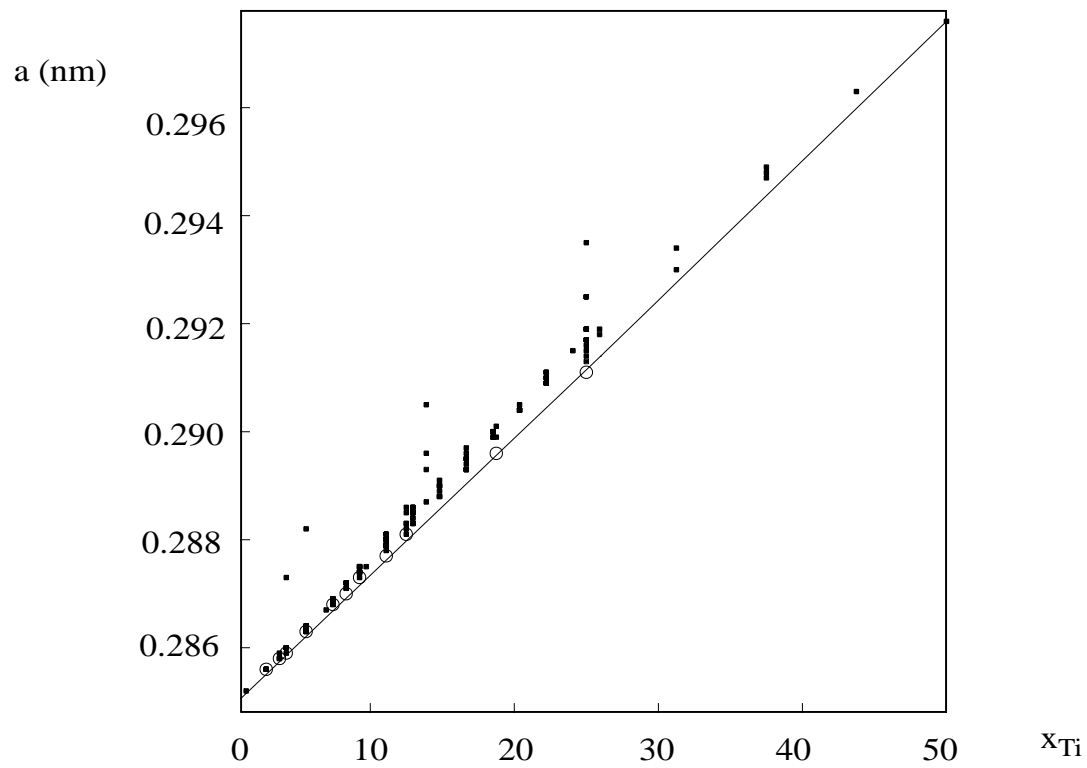
Fig. 8: Lattice parameter of the computational cell for $Ni_{50}Al_{50-x}Ti_x$ alloys as a function of Ti concentration. The results are for a complete computational cell assuming a 'single-phase' alloy for each composition.

The results of Eq. 15 are also plotted in Fig. 8. Similar expressions (Eqs. (40)-(47) in Ref. 16) can be obtained for the concentration dependence of the bulk modulus and cohesive energy per atom. For example, the bulk modulus for multicomponent alloys is given by the approximate expression

$$B(x_1, x_2, \ldots) = \frac{\left(\sum_i a_i B_i\right)^2}{\sum_i a_i^2 B_i}. \tag{19}$$

Using the values of l from Table 1, together with its definition as a function of E_C, a_e and B_0,

$$l = \sqrt{\frac{E_C}{12\pi q a_e B_0}}, \tag{20}$$

we obtain the following approximate expression for the bulk modulus of NiAl-Ti alloys

$$B(x_{Ni}, x_{Al}, x_{Ti}) = \frac{(685.80 x_{Ni} + 248.88 x_{Al} + 388.87 x_{Ti})^2}{1997.32 x_{Ni} + 794.43 x_{Al} + 1249.44 x_{Ti}} \tag{21}$$

Also, simple rules can be obtained (Eqs. 45-47 in Ref. 16) regarding the deviation of such values to the usually assumed average values. Eq. 19 applies to any multicomponent system where all the constituents are parameterized in the same symmetry as the alloy under consideration. In this work, Ni, Al and Ti are described (Table 1) by their lattice parameter, cohesive energy and bulk modulus in the bcc phase.

While the information provided by studying a large number of candidate configurations at absolute zero temperature provides valuable information on the energetics of the system at hand, it says very little in terms of the effect of temperature and processing on the microstructure of the alloy. In this sense, several numerical tools exist to investigate these issues. In this work, we concentrate on the application of Monte Carlo procedures to perform simulations of Ni-Al-Ti alloys. When added to the results of the previous section, the simulation results should provide a more complete theoretical picture of the microstructural behavior of these alloys.

The Monte Carlo procedure employed in this work is a variant of that used to simulate the Ising system [36]. The computational cell used in all simulations consists of a large number of atoms (1024 in most cases shown in this paper) arranged on a body-centered-cubic lattice. Boundary effects are minimized through the use of periodic boundary conditions in all directions. The choice of the size of the cell results from a compromise between computational economy, convenience in visualizing the results, and the ability to distinguish between all the pertinent physical features of the system. Although the simulations shown correspond to a wide range of temperatures, for simplicity we ignore the lattice parameter dependence on temperature and use the zero temperature predictions discussed in the previous section, as we are mostly interested in ground state effects.

For the (high) initial temperature in every simulation, the computational cell is a random solution, i.e. the Ni, Al and Ti atoms are randomly assigned to each site, in direct proportion to their assigned composition (unless otherwise indicated). No vacancies were allowed in the majority of simulations reported in this work, though their incorporation does not present any added

degree of difficulty, as will be demonstrated shortly. Most of the simulations shown correspond to a process where a sequence of decreasing temperatures (the `cascade') is chosen, where the system is allowed to equilibrate sequentially at each temperature. This simulates the `slow cooling' of the actual alloy, starting from a high temperature disordered solid solution. The equilibration procedure involves the random selection of a pair of atoms and their subsequent reversal in position. The reversal in chemical identity is accepted or rejected using the Metropolis criterion where, for a given temperature, an exchange is accepted if it lowers the energy or assigned a probability $exp(-\Delta E/kT)$, where k is Boltzmann constant and ΔE is the change in BFS energy between the configurations after and before the switch. The number of switches allowed is set as an input parameter and it determines, together with the difference in temperature between two successive steps in the simulation, the simulated cooling rate of the sample. A large number of switches can be considered equivalent to a longer stabilization time, which together with small changes in temperatures simulate a slower cooling rate. In this calculation we ignored the dependence of the lattice constant with temperature, therefore temperature enters into the calculation only through the Metropolis criterion. After the system has achieved equilibrium (based on the total energy of the computational cell), various properties of the system are computed and averaged and then the simulation proceeds to the next temperature decrement. The properties calculated include the average energy of the cell, the specific heat, and bond correlations.

While these simulations do not attempt to mimic the detailed dynamics of the equilibration process, they do offer a qualitative view of the effects of rapid versus slow cooling of the system. The cooling rate (that is, the size of the steps between the various temperatures considered in the cascade) is of critical importance in determining the final state of the system. Slow cooling results in a highly-ordered low-temperature state, while rapid cooling results in a more disordered mate-
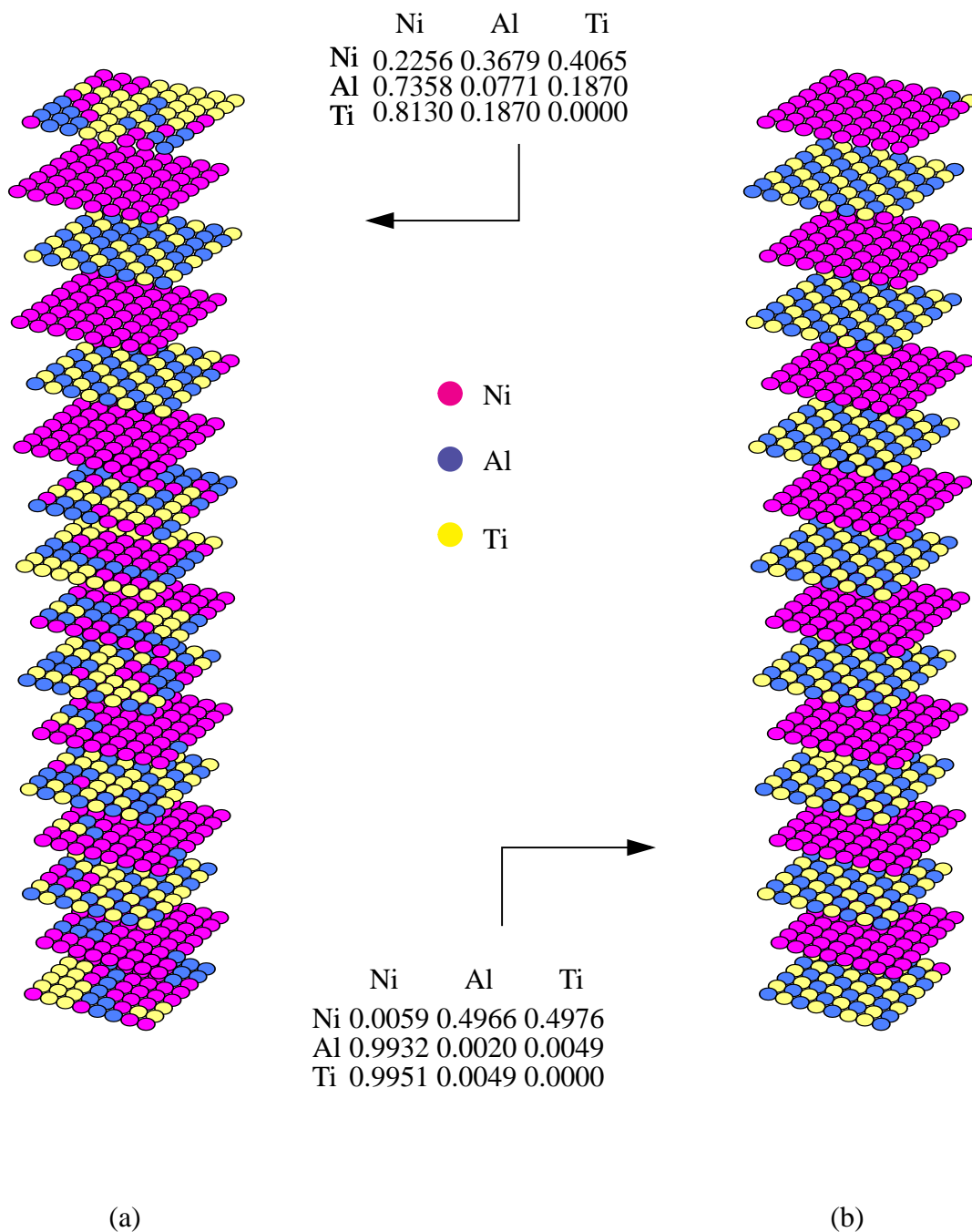
	Ni	Al	Ti
Ni	0.2256	0.3679	0.4065
Al	0.7358	0.0771	0.1870
Ti	0.8130	0.1870	0.0000

● Ni

● Al

● Ti

	Ni	Al	Ti
Ni	0.0059	0.4966	0.4976
Al	0.9932	0.0020	0.0049
Ti	0.9951	0.0049	0.0000

(a)   (b)

Fig. 9: Final structures of a Monte Carlo/Metropolis/BFS simulation on a 1024 atom cell of a Ni-25Al-25Ti alloy. Both (initially random) final states are obtained by lowering the temperature in different ways: Fig. 9.a shows the final geometry for a rapid cooling process, where the final temperature is reached by 'freezing' the initial, high temperature, state. Fig. 9.b is obtained by slowly lowering the temperature in 100 K intervals and allowing the cell to equilibrate, until the final temperature is reached ('cascade' process) at room temperature. The inset includes the coordination matrix for the final state of the simulation: the element ij in this matrix indicates the probability that an atom i has an atom of species j as a nearest-neighbor. The labels i,j take the values 1, 2 and 3, corresponding to Ni, Al and Ti.

rial often containing antiphase boundaries. As with actual processing, the temperature treatment of the sample is essential in determining the final state. It is to be expected that the slow cascade processes, used in most of our calculations, will result in highly ordered compounds. In contrast, sudden cooling of the sample will result in regions of disorder often in the form of antiphase boundaries . It is also possible that additional phases - like the ones described in Fig. 7 and discussed in the previous section - might also appear with a frequency proportional to the difference in energy of formation with respect to other structures (such information can be obtained from the 'static' analysis described in the previous section). The presence of these higher energy structures in the fast cooled sample can arise if quenching of the sample `freezes' specific domains within the cell, whose seed is already present in the initial disordered state.

An example of the effect of cooling rate on structure is shown in Fig. 9 which includes the results of two separate simulations for an alloy with a bulk composition equivalent to Ni_2AlTi, both starting from the same random state at high temperature. To facilitate the visual interpretation of the results, the 1024-atom cubic cell is stretched along the <001> direction. The rapidly cooled cell, shown in Fig. 9.a, is characterized by order and disorder features. There is a clear trend towards separation of Ni-rich and Ti-Al alternating planes, as well as some indication of Heusler ordering in about half the sample. The lower half of the cell shows a noticeable degree of disorder and even the existence of some energetically unfavorable situations, mostly in regions of large Ti or Al concentrations. Fig. 9.b, in contrast, shows the results of a cascade process that had finer steps between temperatures (slow cooled). Even though the final temperature was the same as in the previous case (room temperature), this cell displays almost perfect Heusler ordering. Most of the antisite defects present in this sample are eliminated after subsequent re-heating and slow re-cooling - a second cascade - which results in an almost ideal Heusler phase with a few antisite atoms.
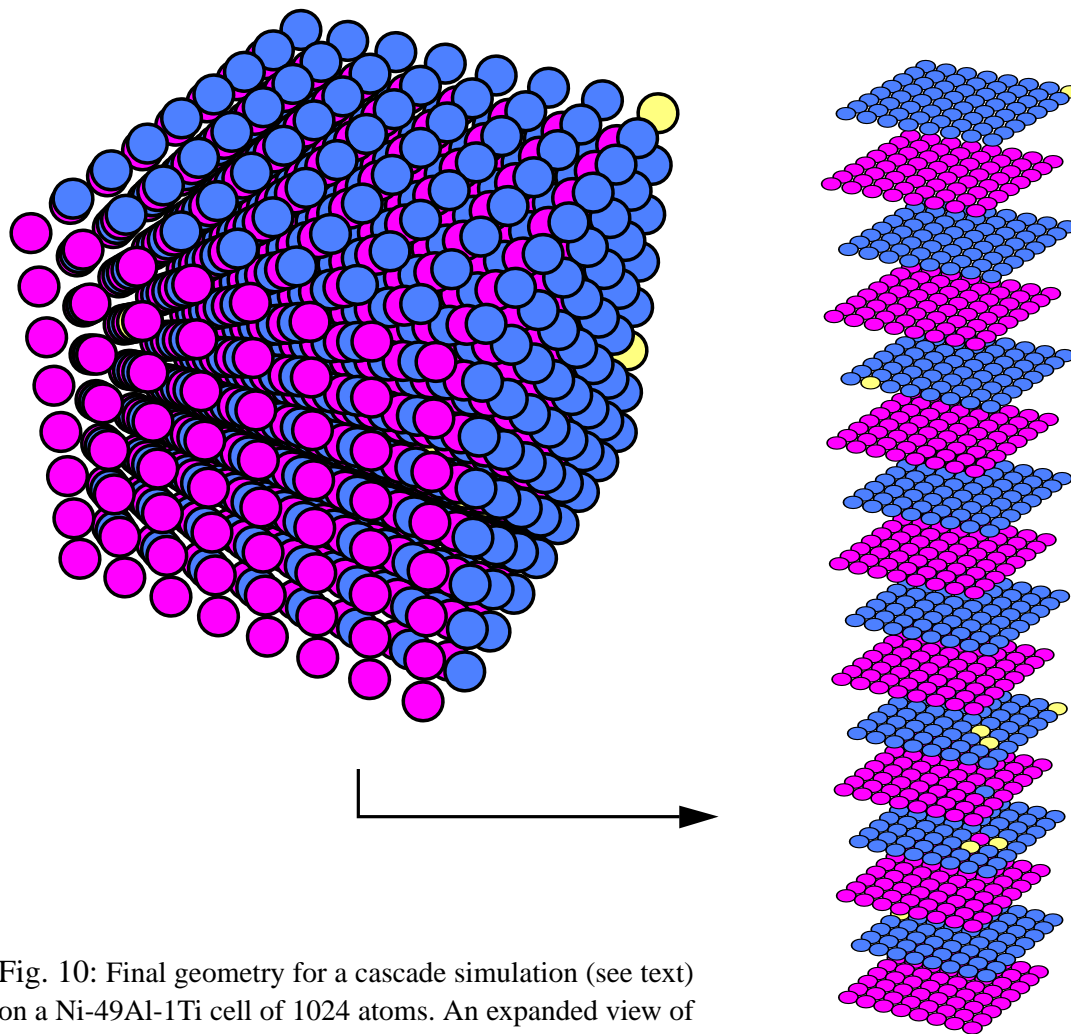
Fig. 10: Final geometry for a cascade simulation (see text) on a Ni-49Al-1Ti cell of 1024 atoms. An expanded view of the cell is also shown.

Figure 10 displays similar results for the slow cooling of a $Ni_{50}(Al,Ti)_{50}$ alloy with 1 at. % Ti. Starting with a random alloy at high temperature, the slowly cooled sample settles into a perfect B2 NiAl ordering with Ti atoms in Al sites. However, no trend toward precipitate formation is seen at this concentration, consistent with the configurational analysis described in the previous section.

Figure 11 shows results for a $Ni_{50}(Al,Ti)_{50}$ alloy with 5 at. % Ti for two different random computational cells. The first three cells in Fig. 11 show the final results of three consecutive
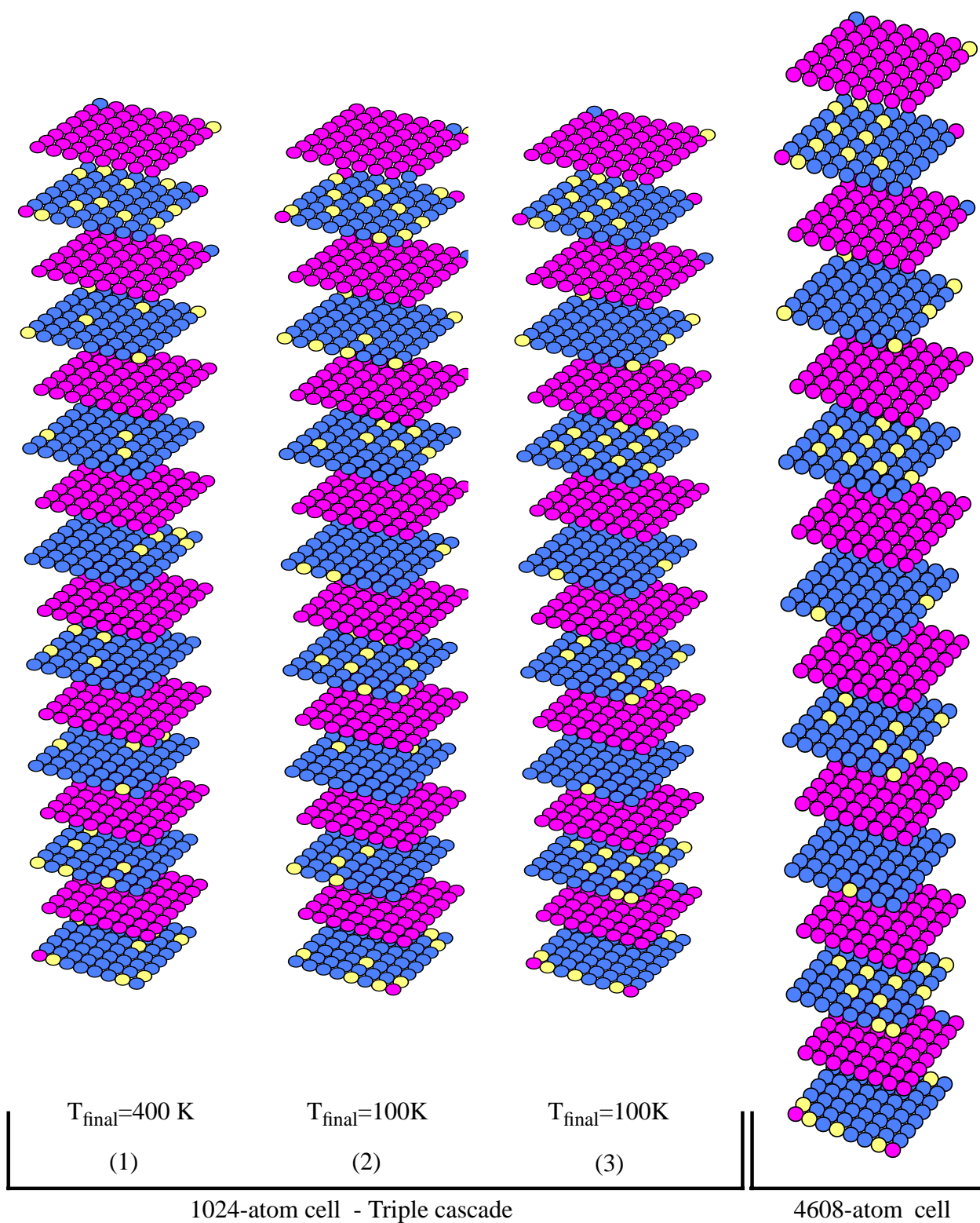
Fig. 11: Results of three consecutive temperature cascades on a Ni-45Al-5Ti 1024-atom computational cell. The fourth column corresponds to a single cascade calculation on a larger (4608 atoms) cell.

Within the figure:

T_{final}=400 K

T_{final}=100K

T_{final}=100K

(1)

(2)

(3)

1024-atom cell - Triple cascade

4608-atom cell

temperature cascades on the same sample, each showing a higher degree of short range order relative to the previous one. A multiple-cascade process consist of consecutive cascades where the final state of a given cascade becomes the initial state of the following one, except for the first cascade where the initial state is a random distribution of atoms. The last cell displays the results of a single temperature cascade for a large (4608 atoms) cell, showing essentially the same features observed in the smaller cell, thus ruling out microstructural effects based on cell size. Since this concentration is near the accepted solubility limit for Ti in NiAl, a larger cell allows for a closer examination of the final state and the possibility of precipitate formation. In this case, the Ti atoms actually display three different types of behavior, as seen in the last column in Fig. 11, which corresponds to the final temperature (T = 400 K): 1) the formation of Heusler precipitates, more clearly seen if the periodicity of the cell is taken into account, 2) Ti atoms in solid solution in the NiAl matrix with preference for the Al-sublattice, and 3) the distribution of Ti atoms following the alternative to Heusler ordering depicted in Fig. 7.b (atoms located in alternate sites along rows parallel to the edges of the sample) in regions often adjacent to Heusler precipitates. Also, a few Ni antisite atoms are seen. While it might prove to be a premature conclusion, it is noticeable that in the final state the antistructure Ni atoms seem to `attract' Ti atoms to their vicinity in the Al plane, creating a Ti-rich interphase with the NiAl matrix. This effect, while visible in the results of the simulation, could be also due to the limitation imposed by forcing the lattice parameter to remain constant during the simulation. This restriction could induce an unrealistic strain in the calculational cell that could eventually drive Ti atoms to the interphase in order to compensate for such effect.

Similar structures are observed in a Ni-40Al-10Ti alloy which has undergone a double-cascade process (Fig. 12). In this type of process, an initially random cell is cooled to a given tamper-
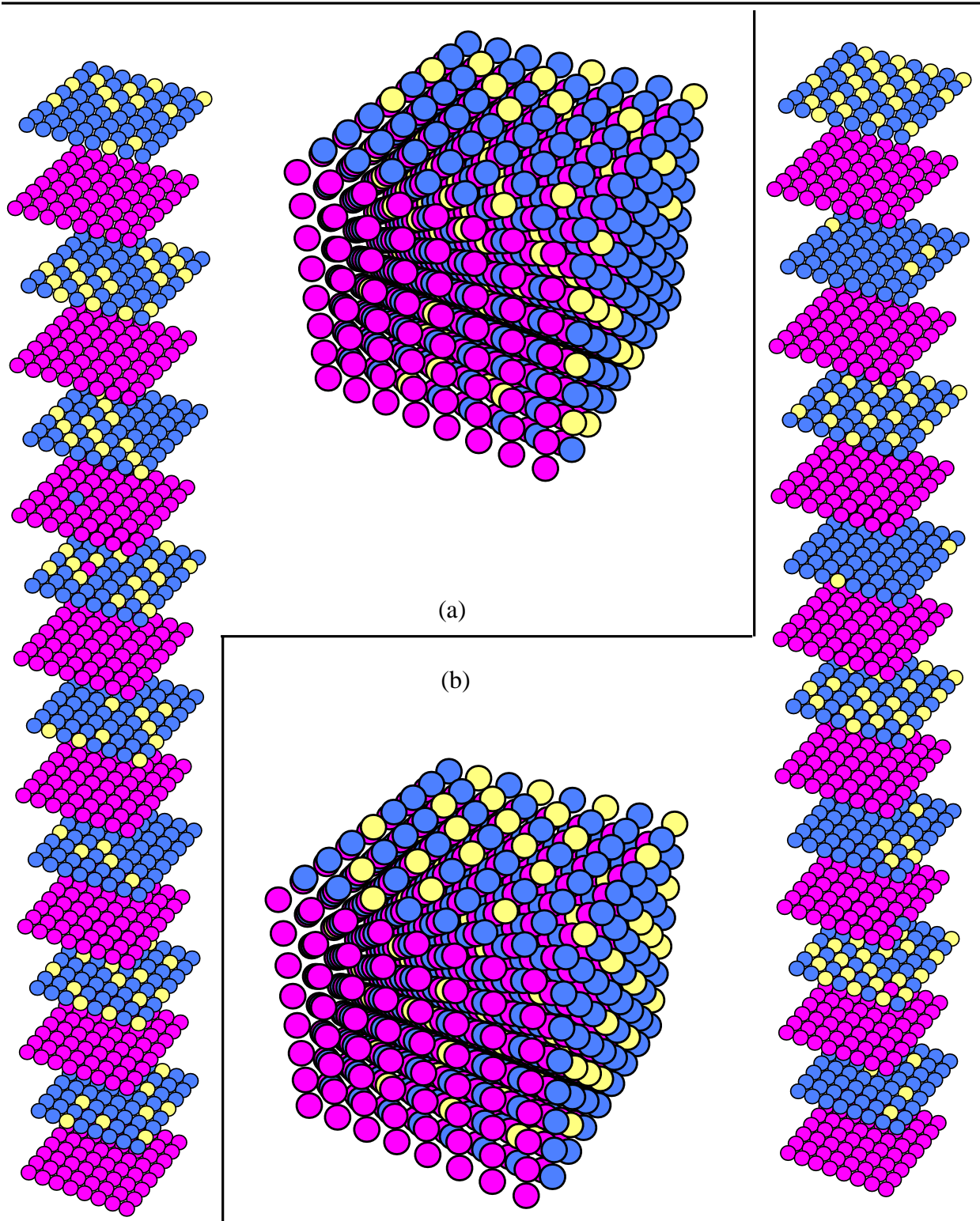
Fig. 12: Final geometry for a double cascade process on a Ni-40Al-10Ti 1024-atom cell. (a) The first expanded cell results from being slowly cooled at equal temperature intervals from an arbitrary high temperature. (b) Then this cell is re-heated and slowly cooled again, reaching the final state shown in the second cell.

ature and then used as the initial state of a new cascade process. At the end of each cascade, the formation of Heusler precipitates (characterized by the chains of Ti atoms along <110> in the Al planes) is clearly observed. In spite of the re-heating and re-cooling of the sample, the Heusler precipitates reappear proving that the dominant effect of sufficient additions of Ti to Ni-rich NiAl is the formation of such precipitates. Some of the other features pointed out in Fig. 11 are also featured in the 10 at. % Ti case: the solid solution of Ti atoms in the matrix, and the presence of an occassional antistructure Ni atom in the Al sublattice, with an apparent clustering of Ti atoms in the vicinity. Also, some Ti atoms following the alternative ordering scheme previously discussed are clearly seen.

Finally, we comment on the role of vacancies on the microstructure of the alloys studied. So far, all the examples shown ignore the presence of vacancies. If vacant sites are allowed in the calculation, it is found that none of the essential microstructural features discussed earlier are affected to any significant degree. However, the results show clear indication of vacancy clustering in such a way that inner Al surfaces are created. This is not surprising, given the large size of Al atoms and the low surface energy of Al, both features conducive to the formation of Al surfaces. Moreover, due to the tendency of vacancies to coalesce, Ni antistructure atoms are then found in the vicinity of vacancy clusters. Some of the unfavorable Ni-Ni bonds thus created are compensated by the migration of some Ti atoms to Ni sites creating favorable Ti-Al bonds.

EXPERIMENTAL ANALYSIS OF NiAl-Ti ALLOYS

Three NiAl single crystal alloys (Ni-47Al-3Ti, Ni-45Al-5Ti and Ni-43Al-7Ti) were grown by a Bridgman technique at the University of Florida. The ingots were homogenized for 32 hrs. at

1644 K, aged for 6 hrs. at 1255 K, and slowly furnace cooled from the aging temperature. The

purpose of this heat treatment was to produce a low temperature 'equilibrium' microstructure that

would best correspond to the ground state conditions modeled under the BFS method. Samples

for transmission electron microscopy (TEM) were prepared from 3 mm diameter cylinders elec-

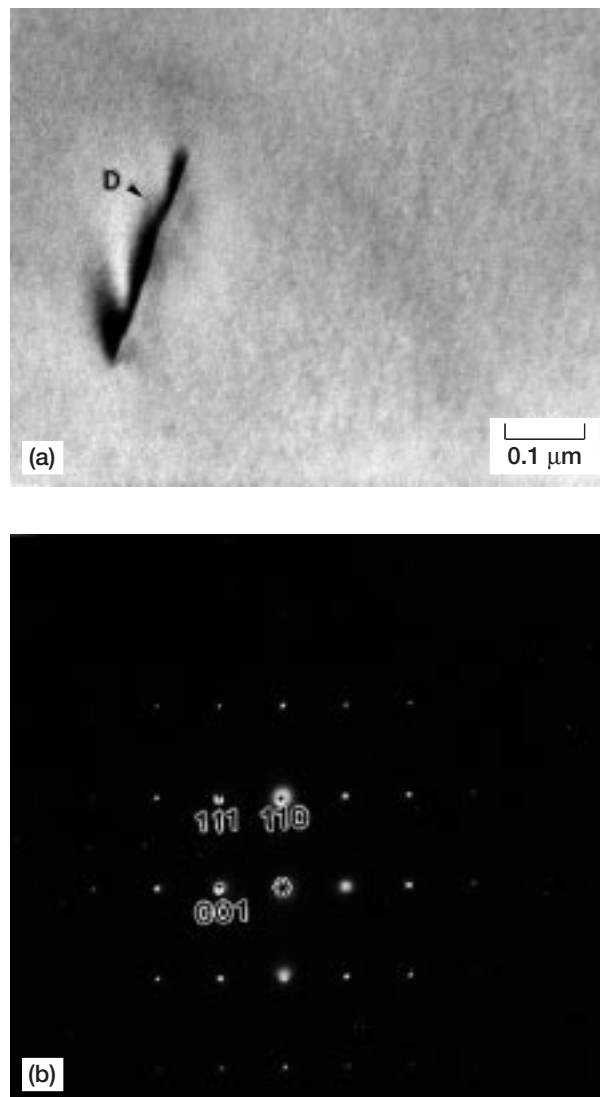tro-discharge machined from the heat treated ingots. Slices sectioned from the cylinders were

Fig. 13: (a) Bright-field TEM image of the microstructure of the Ni-47Al-3Ti alloy and (b) corresponding
<110> SADP. The only features observed in the alloy are an occasional <100> dislocation marked 'D' on
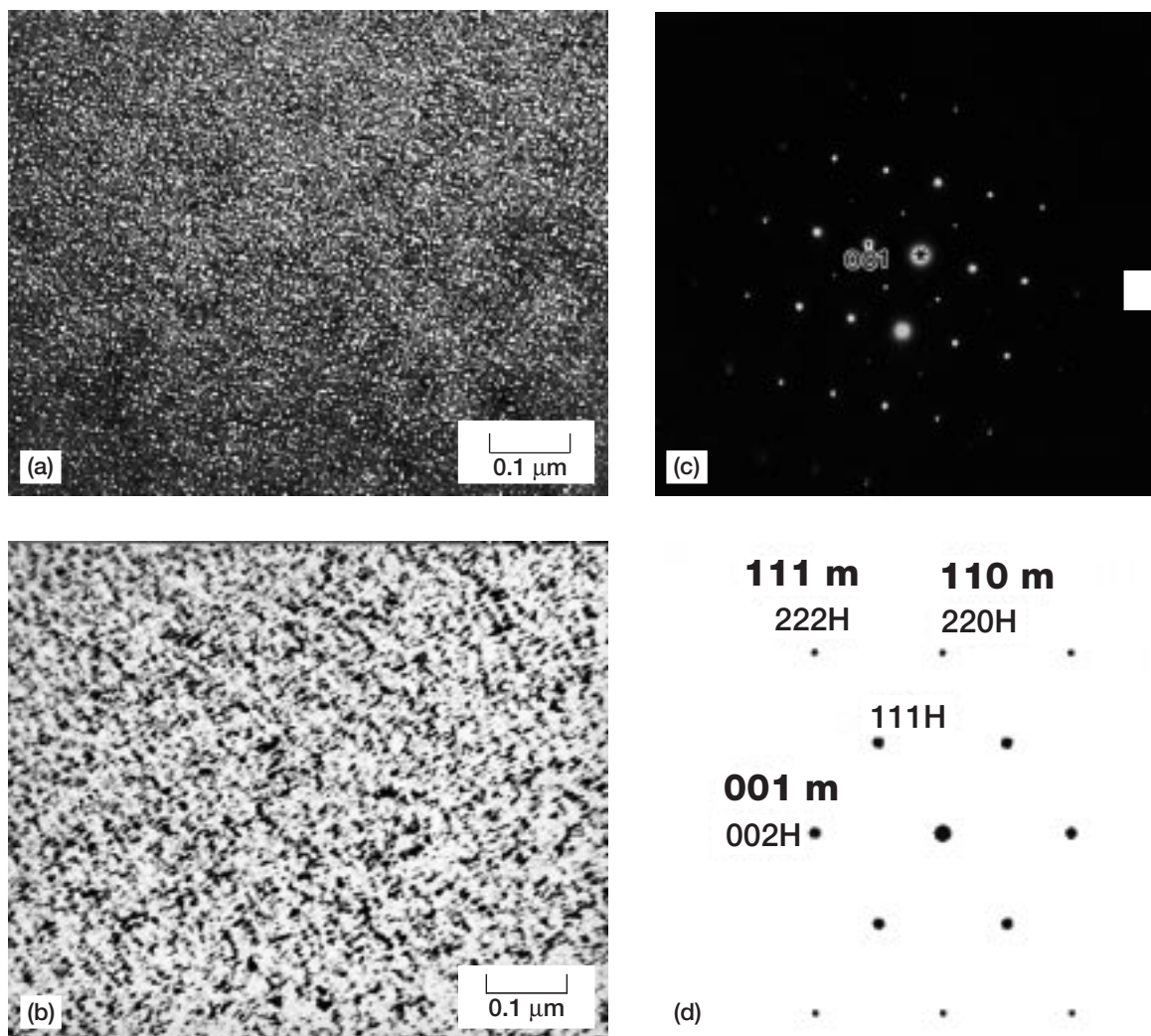(a).

Fig. 14: (a) Bright-field and (b) dark-field TEM image of the Ni-45Al-5Ti alloy showing precipitation of fine Heusler particles, (c) the corresponding SADP and (d) an indexed, simulated pattern.

mechanically ground and electrochemically thinned in a twin-jet Tenupol-3 polisher. Microstructural (bright-field/dark-field) and diffraction analysis were conducted in a Phillips 400T TEM equipped with a double tilt goniometer.

Fig. 13.a shows a brightfield image of the Ni-47Al-3Ti alloy. Except for an occasional dislocation, the microstructure is very clean and featureless and shows no sign of any second phase pre-
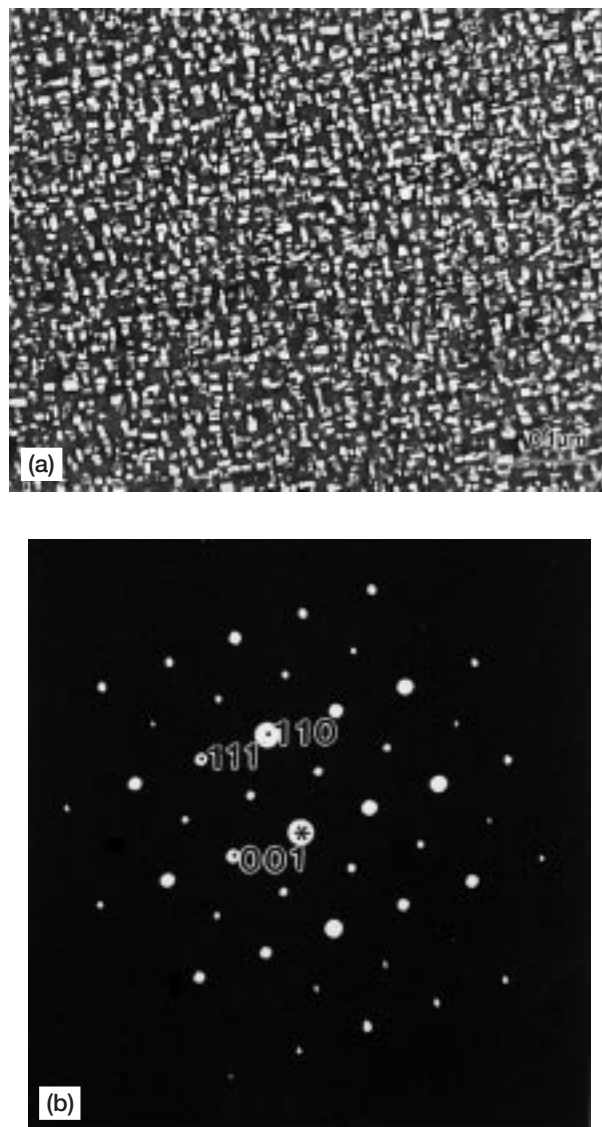

Fig. 15: (a) Dark-field TEM image of the Ni-43Al-7Ti alloy showing dense precipitation of rectangular-shaped Heusler precipitates and (b) the corresponding SADP .

cipitation. This is confirmed in the corresponding <110> zone-axis selected area diffraction pattern (SADP), presented in Fig. 13.b, which shows only the NiAl matrix spots and no extra diffraction features (spots or streaking) due to precipitation.

In contrast, Fig. 14.a shows a bright-field image of the Ni-45Al-5Ti alloy after the same thermal treatment. Precipitation of a high density of extremely fine second-phase particles can be clearly seen, especially in the dark-field image shown in Fig. 14.b, where the precipitates appear bright on a black background. The corresponding <110> SADP in Fig. 14.c shows distinct extra spots which were indexed to a fcc crystal structure with lattice parameter $a_0 = 0.586$ nm, corresponding to the Ni_2AlTi (Heusler) phase. From the crystallographic information revealed from the diffraction pattern (schematically illustrated and labeled in Fig. 14.d), it can be seen that the Ni_2AlTi phase nucleates with a cube-on-cube orientation relationship with the NiAl matrix, i.e. $[110]_{NiAl}//[110]_{Ni2AlTi}$ and $(001)_{NiAl}//(001)_{Ni2AlTi}$. Due to the fine size of the precipitates, 1-5 nm, and the small lattice misfit between these two phases, on the order of 1.5 %, the precipitates are coherent with the matrix resulting in significant coherency strains around the particles, as seen in the bright-field image in Fig. 14.a.

Figure 15 shows a dark-field TEM image of the Ni-43Al-7Ti alloy after the same heat treatment. Precipitation of a high density of well defined and coherent Heusler precipitate plates ranging in size between 10-50 nm can be clearly seen. While the precipitates are on average 10 times larger than those in the Ni-45Al-5Ti alloy, due to the small lattice misfit between the precipitate phase and the NiAl, most of the plates are still coherent with the matrix. Fig. 15.b shows the corresponding SADP.

DISCUSSION

In exploiting the computational simplicity of the BFS method in calculating the energetics of various alloy structures, it must be understood that the technique does not automatically provide the ground state configuration of a particular alloy but depends on the inclusion of that configuration in the catalogue of configurations selected for study. For reference in this and future studies, the present catalogue of configurations has been defined in the Appendix. Returning one last time to the issue of completeness of this set of configurations, Fig. 4 can be used as a clear example of how an occasional omission in the predetermined catalogue can be easily detected and corrected as the large size of the set provides enough statistical information to detect trends and patterns and therefore, infer what configurations might be missing. Had one of the energetically favorable configurations been left out of the original set, the omission would have been noticed as a `discontinuity' in the plot shown in Fig. 4.b. For example, had the Ni_2AlTi Heusler phase (denoted with a circle in Fig. 4.b) not been included in the set, it would have been easily inferred by observing the series of states indicated with open circles, leading to the prediction of such a phase as the ground state for that concentration. In fact, the analytical BFS results for the 25 at. % Ti alloy not only suggest but confirm the $L2_1$ structure as the ground state for Ni_2AlTi. Furthermore, the Monte Carlo-Metropolis simulations provide only the ground state configuration and serve as a complementary technique and check on the analytical approach.

The use of this survey method for studying the energetics of various alloy systems provides one with significant information on not only the ground state structure of a particular alloy but relates general trends in the energy of formation and lattice parameter to changes in concentration and atomic distribution. It also has the important additional advantage of being able to identify

metastable structures or configurations with energy close to that of the ground state, which may have a high probability of appearing in the alloy depending on the actual processing conditions. We note also that Monte Carlo simulations complement the use of our survey method to obtain ground state structures.

One of the more significant results of this investigation is the successful application of the BFS method to the determination of the solubility level of a ternary addition to an ordered inter-metallic compound, in this case Ti in NiAl. The results of static calculations, shown in Fig. 4, suggested that the solubility of Ti in NiAl is close to 5 at. %. This was experimentally verified by examining the microstructure of three NiAl-Ti alloys, where it was found that Ni-47Al-3Ti was a complete solid-solution alloy with no second-phase precipitation, and the nucleation of a high density of Ni_2AlTi precipitates appeared only in NiAl alloys containing 5 or more at. % Ti. Although the calculation of minimum energy ground state configurations via the BFS method was performed at 0 K and the experimental results were obtained at room temperature, the microstructure of these high-melting point ordered alloys is not expected to be different at these low temperatures. Moreover, the Monte Carlo simulations included in this work verify this point. Another useful result of the BFS calculations is the ability of the method to predict the atomic structure of the second phase particles and the lattice parameters of all the constituent phases. Both the static and Monte Carlo simulations were able to predict the correct atomic configuration of the resulting second phase particles, i.e. Ni_2AlTi (Heusler phase), in NiAl-Ti alloys. Based on these calculations, the lattice parameter of the Heusler phase was found to be 0.5828 nm, which is in close agreement with the average value of 0.5876 nm reported for the Ni_2AlTi structure [36]. The lattice parameter of the corresponding solid solution NiAl-Ti alloy was calculated to be 0.2865 nm. Thus, based solely on the BFS analytical approach, the lattice mismatch between NiAl and

Ni$_2$AlTi is found to be 1.7 %, which is very close to the approximately 1.5 % misfit obtained experimentally via TEM. A controlled mismatch between phases is one of the major design criteria in almost all high temperature alloys. Therefore, the ability to model not only the correct second phases but also the resulting lattice mismatch is a significant breakthrough in the computational design of high temperature alloys.

An additional significant contribution of this analysis is the ease with which the site occupancy of a third element can be determined in a structure. Knowledge of site occupancy of an alloying element is an important and necessary piece of information in understanding the defect structure and its impact on mechanical properties [37]. In the case of NiAl-Ti alloys studied here, the BFS method was able to correctly predict the site occupancy of Ti in the NiAl lattice with additional information on the overall substitutional scheme, as seen in Fig. 6. The preference of a Ti atom to occupy an Al site in Ni-rich NiAl is well established [4] and, in fact, all the empirical alloy development programs start with this basic assumption.

The most common experimental techniques for determination of site occupancy are ALCHEMI (atom location by channeling enhanced microanalysis) [38] and APFIM (atom-probe field ion microscopy) [39]. However, these are often tedious and very involved procedures and in the case of the former there are a number of complications which make the technique relatively inaccurate [40]. The ability and ease to analytically determine the site occupancy of alloying additions, as proven by the BFS simulations shown in this work, is not only beneficial to an alloy developer, but is a boon to those trying to determine the mechanistic behavior of ordered alloys. Moreover, the methodology used in this work is easily applicable to more than one alloying element, which allows for a clear understanding of the interaction between the different alloying additions [41], as will be demonstrated in future articles.
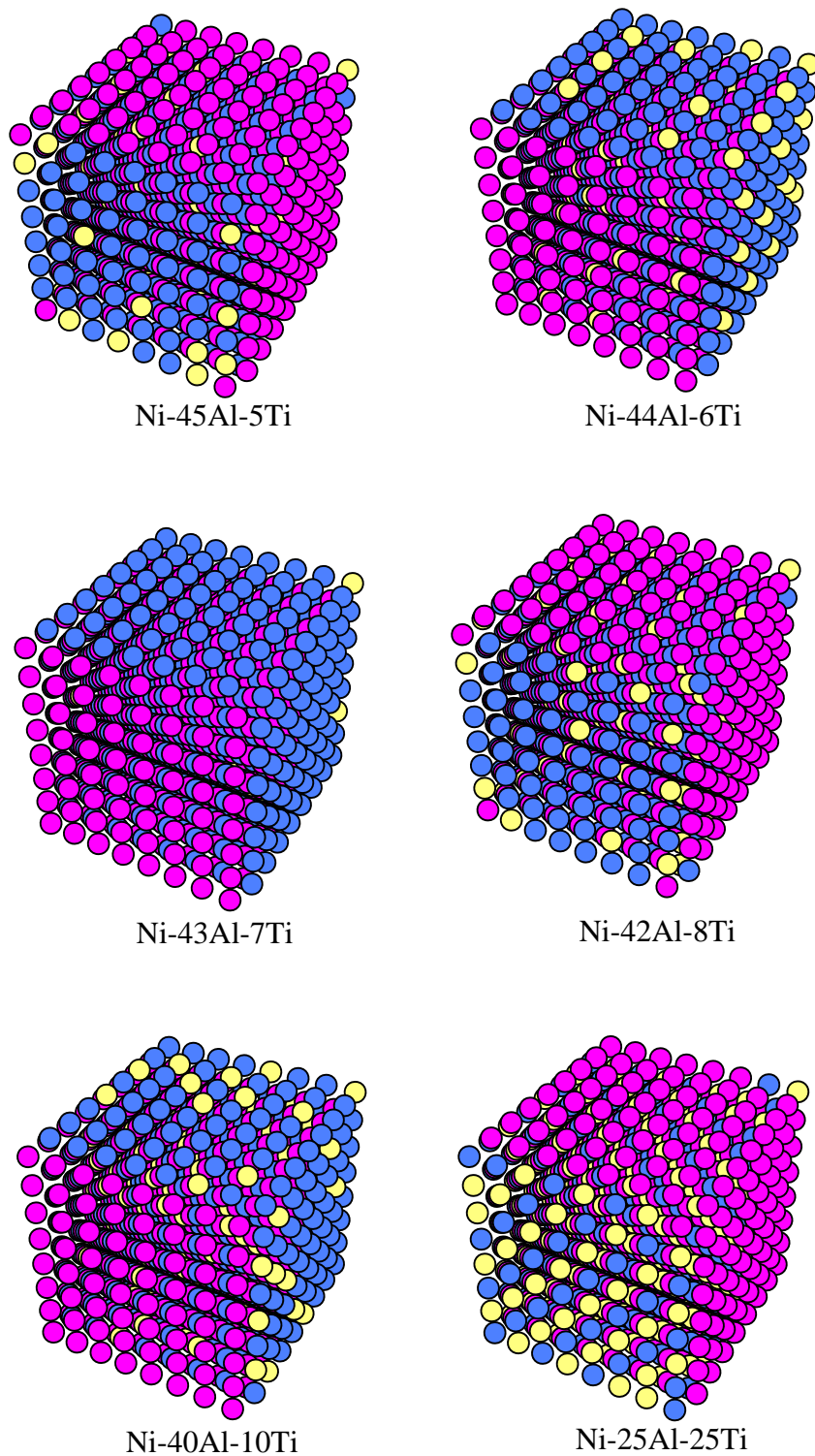
Ni-45Al-5Ti

Ni-44Al-6Ti

Ni-43Al-7Ti

Ni-42Al-8Ti

Ni-40Al-10Ti

Ni-25Al-25Ti

Fig. 16: Summary of final states for Monte Carlo/Metropolis cascade processes for $Ni_{50}Al_{50-x}Ti_x$ alloys (x = 1, 5, 6, 7, 8, 10, 25) for 1024-atom cells.

While a great deal of structural information has been derived from the static calculations, they do not provide much information in regards to the effect of temperature and processing conditions on microstructure. Therefore, to complement the static calculations and further our understanding of these alloys, Monte Carlo procedures were used to perform simulations on the Ni-Al-Ti alloys. These results are summarized in Fig. 16. Figure 16 shows the 1024-atom computational cell for the final states of temperature cascades for a number of different concentrations, some of these have been discussed in detail previously.

The results show that Heusler formation is apparent beyond the solubility limit for Ti. But as in any real system, there is also a statistical chance for the development of other structures at a rate based on differences in energy between them and the ground state. In this case, the alternative ordering scheme shown in Fig. 7.b and an occasional Ni-antistructure atom are evident. The abundance of this alternative type of ordering can be easily explained in terms of our earlier discussion of nearest and next-nearest-neighbor coordination. With such small energy differences involved, when a Ti atom has the choice of occupying an Al site in a Monte Carlo calculation, the difference between a Heusler site and a site belonging to the alternate ordering scheme makes the probability at high temperatures almost identical between the two sites. Therefore, once a Ti atom is `trapped' in an alternative ordering site, its likelihood to migrate further to form a Heusler arrangement with decreasing temperature diminishes. With increasing Ti concentration, the energetically favorable Heusler site becomes more prevalent and the formation of Heusler precipitates is clearly favored due to the larger number of energetically favorable bonds thus created. In addition, the number of temperature decrements within the cascade - the cooling rate of the alloy - influences the density of these higher energy structures observed in the final microstructure.

CONCLUSIONS

The BFS method has been successful in predicting the solubility limit, structure of the second phase particles, lattice mismatch between the alloy matrix and the precipitating phases, atomic size factors, and preferred site occupancy of the alloying additions. These results have proven that almost all the necessary parameters needed for a purely analytical alloy design approach are now within reach. The present results provide confidence in the BFS technique, the authenticity of the input parameters used (Tables 1 and 2) and the approach used for obtaining parameters by use of ab-initio methods, which removes the limitations imposed by the otherwise required experimental data base. The results also provide an energetic description of the detailed microstructure of the NiAl-Ti system. The real asset of the BFS method would be to model more complex systems such as ordered binary alloys containing two or more alloying additions, required for modelling alloys needed in practical applications, which is in progress. Work in this area will be presented in future papers.

ACKNOWLEDGMENTS

REFERENCES

1. Noebe, R. D., Bowman, R. R. and Nathal, M. V., Inter. Mater. Rev. 38 (1993) 193.

2. Walton, W. S., Field, R. D., Dobbs,J. R., Lahrman D. F. and Darolia,R., in Structural Intermet-alics, Darolia R. et al. eds., The Minerals, Metals and Materials Society, 1993, pp. 523-532; Daro-lia, R., JOM 43 (1991) 44; Darolia, R. and Walton W. S. in Structural Intermetallics 1997, Nathal, M. V. et al. eds., The Minerals, Metals, and Materials Society, 1997, pp. 585-594.

3. Darolia, R., Walston W. S. and Nathal, M. V., in Superalloys 1996, Kissinger, R. D. et al. eds., The Minerals, Metals and Materials Society, 1996, pp. 561-570.

4. Kitabjian,P. H., Garg, A., Noebe, R. D. and Nix, W. D., Metall. Mater. Trans. (1998) (in press); Noebe, R. D., and Walston, W. S., in Structural Intermetallics 1997, Nathal, M. V. et al. eds., The Minerals, Metals, and Materials Society, 1997, pp. 573-584.

5. Mills, M. J., Gibeling, J. C. and Nix, W. D., Acta Metall. 33 (1985) 1503; Krachler, R., Ipser, H., Sepiol, B. and Vogl, G., Intermetallics 3 (1995) 83, and references therein.

6. Hosoda, H., Inoue, K., Mishima, Y., Mat. Res. Soc. Symp. Proc. 364 (1995) 483; Fu, C. L., Ye, Y. Y., Yoo, M. H. and Ho, K. M., Phys. Rev. B 48 (1993) 6712, and references therein.

7. Bozzolo, G., Ferrante, J., Noebe, R. D. and Amador, C., Scripta Mater. 36 (1997) 813; Fu, C. L. and Zou, J., Mat. Res. Soc. Symp. Proc. 364 (1995) 91.

8. Kao, C. R., Pike, L. M. , Chen, S. -L. and Chang, Y. A., Intermetallics 2 (1994) 235, and refer-ences therein.

9. Bozzolo, G., Noebe, R. D., Ferrante, J., and Amador, C., J. Computer-Aided Mater. Design

10. Bozzolo and J. Ferrante, J. Computer-Aided Mater. Design 2 (1995) 113.

11. Bozzolo, G., Ferrante, J. and Smith, J. R., Phys. Rev. B 45 (1992) 493.

12. Bozzolo, G. and Ferrante, J., Phys. Rev. B 45 (1992) 12191.

13. Bozzolo, G. and Ferrante, J., Ultramicroscopy 42/44 (1992) 55.

14. Bozzolo, G., Ibanez-Meier, R., and Ferrante, J., Phys. Rev. B 51 (1995) 7207.

15. Bozzolo, G., Good, B. and Ferrante, J., Surf. Sci. 289 (1993) 169.

16. Bozzolo, G. and Ferrante, J. , Phys. Rev. B 50 (1994) 5971.

17. Smith, J. R., Perry, T., Banerjea, A., Ferrante, J. and Bozzolo, G., Phys. Rev. B 44 (1991)

6444.

18. Rose, J. H. , Smith, J. R. and Ferrante, J. , Phys. Rev. B 28 (1983) 1835.

19. Andersen, O. K., Postnikov, A. V. and Savrasov, S. Y., Mat. Res. Soc. Symp. Proc. 253

(1992) 37.

20. Kohn, W. and Sham, L. J. , Phys. Rev. 140 (1965) A1133.

25. Polvani, R. S. , Tzeng, W. -S. and Strutt, P. R., Met. Trans. A 7 (1976) 33.

26. Boettinger, W. J., Bendersky, L. A., Biancaniello, F. S. and Cahn, J. W., Maters. Sci. Eng. 98

(1988) 273.

27. Field, R. D., Darolia, R. and Lahrman, D. F. , Scripta Metall. 23 (1989) 1469.

28. Takeyama, M., Liu, C. T. and Sparks, C. J., in Proceedings of International Symposium on

Intermetallic Compounds - Structure and Mechanical Properties - (JIMIS -6), Izumi, O. ed., The

Japan Institute of Metals, 1991, pp. 871-875.

29. Fu, C. L. and Zou, J., Acta Mater. 44 (1996) 1471.

30. Tso, N. C. and Sanchez, J. M., Mat. Res. Soc. Symp. Proc. 133 (1989) 63.

31. Bozzolo,G., Amador, C., Ferrante, J. and Noebe, R. D., Scripta Metall. Mater. 33 (1995) 1907.

32. Kogachi, M., Minamigawa, S. and Nakahigashi, K. , Acta Metall. 40 (1992) 1113.

33. Kitabjian, P. H., and Nix, W. D., Acta mater. 46 (1998) 701.

34. Oh-ishi, K., Horita, Z. and Nemoto, M., Mater. Trans. JIM 38 (1997) 99.

35. Vegard, L., Z. Phys. 5 (1921) 17.

36. Good, B., Bozzolo, G. and Ferrante, J., Phys. Rev. B 48 (1993) 18284.

37. Pearson, W. B. in Handbook of Lattice Spacings and Structure of Metals, Pergamon, New York, 1967.

38. Cotton, J. D., Noebe, R. D. and Kaufman, M. J. in Structural Intermetallics, Darolia, R. et al. eds., The Minerals, Metals and Materials Society, 1993, pp. 513-523.

39. Miller, M. K. and Smith, G. D. W., in Applications of Atom Probe Microanalysis in Materials Science, MRS Bulletin, Volume XIX, No. 7, (July 1994), pp. 27-34.

40. Rossouw, C. J., Forwood, C. T., Gibson, M. A. and Miller, P. R., Phil. Mag. A, 74 (1996) 57.

41. Munroe, P. R. and Baker, I., J. Mater. Res. 7 (1992) 2119.

42. Bozzolo, G., Noebe, R. D., and Honecy, F. S., in Interstitial and Substitutional Effects in Intermetallics, Baker, I., Noebe, R. D., and George, E., eds., The Minerals, Metals and Materials Society, Warrendale, PA, 1998, pp. 341.

APPENDIX

The computational cell is defined in Fig. 3.a. It corresponds to a bcc lattice with 72 sites. The B2 NiAl alloy corresponds to the atomic distribution shown in Fig. 3.a, where Ni atoms are denoted by black disks (labeled 1, 2, 3, ...) and the Al atoms are denoted by open circles (labeled 13,14,15,...). A set of configurations is defined by changing the occupancy of these sites by 1) exchanging an A atom in site n with a B atom in site m (A <-> B) or by 2) substituting an atom B in site m with an atom A that originally was in site n (A -> B).Some of the configurations correspond to smaller versions of the 72 atom cell: those denoted with an asterisk (*) correspond to a cell where atoms 4n (n = 1,...,18) have been eliminated and those configurations denoted with a double asterisk (**) correspond to a fraction of the original cell where only atoms (1,2,5,6,9,10,17,18,25,26,29,30,37,38,41,42) are taken into account. Fig. 3.b shows two examples of the configurations included in the set listed below, corresponding to x_{Ti}= 13.89 and x_{Ti} = 25.00. The Table in this Appendix lists, for each Ti concentration, the different configurations used and their resulting energy of formation and corresponding equilibrium lattice parameter (determined by minimizing the energy of formation). For example, one of the configurations for x_{Ti} = 13.89 (shown in Fig. 3.b) is labeled as: [Al -> Ti](37-48) + Ni(49,60) <-> Al(61,72), indicating that the Al atoms in sites 37 through 48 are replaced by Ti atoms, and that the Ni atoms originally in sites 49 and 60, exchange places with the Al atoms in sites 61 and 72.

The other configuration shown in Fig. 3.b and corresponds to x_{Ti} =25.00. The configuration is labeled as [Al -> Ti] (14,16,17,19,22,24,37,39,42,44,45,47,62,64,65,67,70,72) and indicates that Ti atoms now occupy the listed sites in the Al-sublattice, so that the final configuration corresponds to the Heusler phase shown in Fig. 7.a.

CATALOGUE OF ATOMIC CONFIGURATIONS

x_{Ti}	Configuration	ΔH (eV/atom)	a (A)
0.00	B2	-0.61311	2.848
	Ni(31)<->Al(42)	-0.51543	2.857
	Ni(30,32)<->Al(41,43)	-0.41837	2.866
	Ni(30,32)<->Al(42,43)	-0.41724	2.867
	Ni(30,31)<->Al(42,43)	-0.44122	2.864
1.39	[Al<->Ti](42)	-0.60954	2.852
2.78	[Al<->Ti](42,44)	-0.60634	2.856
	[Al<->Ti](38,44)	-0.60615	2.856
	[Al<->Ti](38,43)	-0.60577	2.856
	[Al<->Ti](42,43)	-0.60243	2.856
3.70	[Al<->Ti](39,66)*	-0.60363	2.858
	[Al<->Ti](37,42)*	-0.60350	2.858
	[Al<->Ti](42,43)*	-0.59918	2.859
4.17	[Al<->Ti](17,39,71)	-0.60258	2.859
	[Al<->Ti](18,38,43)	-0.60195	2.859
	[Al<->Ti](42-44)	-0.59592	2.860
	[Al<->Ti](42,46,47)	-0.59573	2.860
	[Al<->Ti](38,42,46)	-0.59267	2.860
	[Ni<->Ti](50,54,58) + [Al<->Ti](62,66,70)	-0.41575	2.873
5.55	[Al<->Ti](17,37,42)*	-0.59861	2.863
	[Al<->Ti](37,42,47)*	-0.59844	2.863
	[Al<->Ti](15,18,38,43)	-0.59816	2.863
	[Al<->Ti](22,41,63,70)	-0.59527	2.863
	[Al<->Ti](41,42,47)*	-0.59414	2.864
	[Al<->Ti](38,42,43)*	-0.59048	2.864

x_{Ti}	Configuration	ΔH (eV/atom)	a (A)
5.55	[Al<->Ti](38,39,41,42)	-0.58915	2.864
	[Al<->Ti](18,19,42,43)	-0.58637	2.864
	[Al<->Ti](41,-43)*	-0.58630	2.864
	[Ni->Ti](52,56) + [Al -> Ni](65-68)	-0.35182	2.882
6.25	[Al -> Ti](13)**	-0.59975	2.865
6.94	[Al -> Ti](22,41,64,66,72)	-0.59194	2.867
	[Al -> Ti](15,18,38,43,46)	-0.59098	2.867
7.41	[Al -> Ti](14,19,39,42)*	-0.59383	2.868
	[Al -> Ti](14,42,45,67)*	-0.59358	2.868
	[Al -> Ti](14,41,43,70)*	-0.58945	2.868
	[Al -> Ti](15,19,38,42)*	-0.58562	2.869
	[Al -> Ti](37,42,43,66)*	-0.58560	2.869
	[Al -> Ti](17,42,65,67)*	-0.58528	2.869
	[Al -> Ti](38,41,43,46)*	-0.58466	2.869
	[Al -> Ti](38,39,42,43)*	-0.57847	2.869
	[Al -> Ti](18,38,42,46)*	-0.57803	2.869
8.33	[Al -> Ti](15,18,20,38,40,43)	-0.59161	2.870
	[Al -> Ti](38,40,41,43,46,48)	-0.58482	2.871
	[Al -> Ti](20,21,22,46,62,68)	-0.58235	2.871
	[Al -> Ti](17,19,41,43,65,67)	-0.57473	2.872
	[Al -> Ti](17,41,42,43,44,65)	-0.57093	2.872
9.26	[Al -> Ti](14,19,39,42,69)*	-0.58892	2.873
	[Al -> Ti](14,19,22,39,42)*	-0.58465	2.873
	[Al -> Ti](37,42,45,62,70)*	-0.58058	2.874
	[Al -> Ti](14,22,37,39,42)*	-0.58028	2.874
	[Al -> Ti](14,37,39,42)*	-0.57998	2.874

x_{Ti}	Configuration	ΔH (eV/atom)	a (A)
9.26	[Al -> Ti](38,39,42,43)*	-0.57376	2.874
	[Al -> Ti](17,19,42,65,67)*	-0.57312	2.875
	[Al -> Ti](39,42,43,45,46)*	-0.57264	2.875
	[Al -> Ti](38,41,42,43,46)*	-0.56647	2.875
9.72	[Al -> Ti](13,15,18,38,41,43,46)	-0.58443	2.874
	[Al -> Ti](17,23,39,47,61,66,72	-0.58159	2.875
11.11	[Al -> Ti](13,15,18,20,38,40,41,43)	-0.58468	2.877
	[Al -> Ti](38,41,46,61,66,69)*	-0.57593	2.878
	[Al -> Ti](13,18,38,41,43,66)*	-0.57552	2.878
	[Al -> Ti](42,44,46,48,65,67,69,71)*	-0.57302	2.879
	[Al -> Ti]((13,21,38,46,63,71)*	-0.57235	2.879
	[Al -> Ti](17,19,22,37,39,67)*	-0.57197	2.879
	[Al -> Ti](13,17,19,42,45,66)*	-0.57157	2.879
	[Al -> Ti](14,18,37,39,47,66)*	-0.56802	2.879
	[Al -> Ti](19,20,37,39,41,44,66,67)	-0.56679	2.879
	[Al -> Ti]((15,19,38,42,61,64,69,72)	-0.56662	2.879
	[Al -> Ti](38,41,42,43,46)*	-0.56176	2.880
	[Al -> Ti](13,17,21,63,67,71)*	-0.56116	2.880
	[Al -> Ti](37,38,42,43,45,47)*	-0.56050	2.880
	[Al -> Ti](13,17,18,21,42,66)*	-0.55817	2.880
	[Al -> Ti](37,39,41,42,43,46)*	-0.55792	2.880
	[Al -> Ti](18,19,22,23,42,43,46,47)	-0.55335	2.881
	[Al -> Ti](41,42,43,44,65,66,67,68)	-0.55220	2.881
12.50	[Al -> Ti](13,38)**	-0.58300	2.881
	[Al -> Ti](13,42)**	-0.58000	2.881
	[Al -> Ti](13,15,18,20,38,40,41,43,46)	-0.57789	2.881

x_{Ti}	Configuration	ΔH (eV/atom)	a (A)
12.50	[Al -> Ti](13,19,22-24,38,43,62,67)	-0.56031	2.883
	[Al -> Ti](13,14)**	-0.55910	2.883
	[Al -> Ti](38-40,42,44,46-48)	-0.54184	2.885
	[Al -> Ti](14,18,22,38,42,46,62,66,70)	-0.53443	2.886
12.96	[Al -> Ti](38,41,43,46,63,66,69)*	-0.57087	2.883
	[Al -> Ti](13,15,18,38,43,66,69)*	-0.57081	2.883
	[Al -> Ti](18,38,41,46,61,66,69)*	-0.56697	2.883
	[Al -> Ti](13,18,39,42,47,66,69)*	-0.56350	2.884
	[Al -> Ti](19,21,38,41,42,46,47)*	-0.56090	2.884
	[Al -> Ti](18,37,39,42,45,47,66)*	-0.55261	2.885
	[Al -> Ti](14,18,22,37,38,46,47)*	-0.55135	2.885
	[Al -> Ti](18,38,41-43,46)*	-0.54795	2.885
	[Al -> Ti](38,39,41-43,45,46)*	-0.54360	2.886
	[Al -> Ti](38,39,41-43,46,47)*	-0.54099	2.886
13.89	[Al -> Ti](13,15,18,20,21,38,40,41,43,46)	-0.57135	2.885
	[Al -> Ti](15,18,19,38,41,42,44,47,63,69)	-0.55710	2.887
14.81	[Al -> Ti](14,15,17,22,37,43,62,71)*	-0.56300	2.888
	[Al -> Ti](15,18,23,38,43,61,63,66)*	-0.55915	2.888
	[Al -> Ti](14,17,19,22,37,39,42,45)*	-0.55887	2.888
	[Al -> Ti](13,17,18,22,38,41,42,45)*	-0.54781	2.889
	[Al -> Ti](18,19,22,23,41,42,45,46)*	-0.54140	2.890
	[Al -> Ti](13,14,17,18,37,38,41,42)*	-0.53689	2.890
	[Al -> Ti](13,14,18,22,37,38,42,46)*	-0.53537	2.891
16.67	[Al -> Ti](37,39,42,44,45,47,62,64,65,67,70,72)	-0.55922	2.893
	[Al -> Ti](15,18,23,38,41,43,61,66,71)	-0.55407	2.893
	[Al -> Ti](14,19,21,37,39,41,42,46,47)*	-0.54840	2.893
	[Al -> Ti](38,41,43,46,61,63,66,69,71)*	-0.54782	2.893

x_{Ti}	Configuration	ΔH (eV/atom)	a (A)
16.67	[Al -> Ti](14,17,22,39,42,47,61,65,69)*	-0.54745	2.893
	[Al -> Ti](13,23,38,39,42,45,46,61,71)*	-0.54405	2.894
	[Al -> Ti](15,19,23,37,41,45,62,66,70)*	-0.53747	2.895
	[Al -> Ti](39,41,42,45,46,65,66,69,70)*	-0.53216	2.895
	[Al -> Ti](15,19,23,37,39,41,43,45,47,61,65,69)	-0.52729	2.896
	[Al -> Ti](18,37-39,42,45-47,66)*	-0.52317	2.896
	[Al -> Ti](61-63,65-67,69-71)*	-0.51218	2.897
	[Al -> Ti](37-48) + Ni(49-60) <-> Al(61-72)	-0.32156	2.905
18.52	[Al -> Ti](13,18,21,38,39,41,62,67,69,70)*	-0.54339	2.898
	[Al -> Ti](14,17,19,42,61,63,65,67,69,71)*	-0.53964	2.899
	[Al -> Ti](14,17,19,22,42,61,63,66,69,71)*	-0.53938	2.899
	[Al -> Ti](13,17,38,41-43,45,47,66,70)*	-0.52873	2.900
	[Al -> Ti](18,19,38,39,42,43,63,65,66,71)*	-0.52587	2.900
18.75	[Al -> Ti](13,18,38)**	-0.56750	2.896
	[Al -> Ti](13,17,38)**	-0.54137	2.899
	[Al -> Ti](13,14,18)**	-0.52327	2.901
20.37	[Al -> Ti](14,17,19,22,37,39,42,45,65,67)*	-0.52883	2.904
	[Al -> Ti](15,21,22,37,39,41-43,47,65-67)*	-0.52345	2.904
	[Al -> Ti](15,17,18,38,41,43,46,62,65,67,70)*	-0.52307	2.904
	[Al -> Ti](15,18,19,23,37,38,42,46,61,67,70)*	-0.52068	2.904
	[Al -> Ti](13,15,18,37,39,41,42,45,46,61,66)*	-0.51254	2.905
22.22	[Al -> Ti](14,17,19,22,37,39,42,45,47,62,67,70)*	-0.52146	2.908
	[Al -> Ti](13,15,21,23,38,41,43,46,62,65,67,70)*	-0.51472	2.909
	[Al -> Ti](13,18,19,21,38,39,41,42,46,47,66,67)*	-0.51144	2.909
	[Al -> Ti](14,17,18,23,38,39,41,43,45,47,63,67)*	-0.50905	2.909

x_{Ti}	Configuration	ΔH (eV/atom)	a (A)
22.22	[Al -> Ti](13,14,19,38,41-43,45,62,66,67,71)*	-0.50631	2.910
	[Al -> Ti](13,18,37-39,41,43,45-47,66,71)*	-0.50456	2.910
	[Al -> Ti](13,15,17,19,21,23,38,42,46,62,66,70)*	-0.49771	2.911
	[Al -> Ti](13,14,17,18,21,22,37,38,41,42,45,46)*	-0.48996	2.911
24.07	[Al -> Ti](13,15,18,21,38,41,43,46,61,63,66,69,71)*	-0.51303	2.913
	[Al -> Ti](14,18,19,22,37,39,41,43,45,47,62,66,70)*	-0.48968	2.915
25.00	[Al -> Ti](14,17,37,42)**	-0.55583	2.911
	[Al -> Ti](14,16,17,19,22,24,37,39,42) + [Al -> Ti](44,45,47,62,64,65,67,70,72)	-0.52068	2.914
	[Al -> Ti](13,14,37,42)**	-0.50999	2.915
	[Al -> Ti](13,14,41,42)**	-0.50504	2.916
	[Al -> Ti](14,37,38,42)**	-0.49365	2.917
	[Al -> Ti](14,18,37,38)**	-0.48963	2.917
	[Al -> Ti](13,14,17,18)**	-0.47424	2.919
	[Al -> Ni](14,17,37,42)**+[Ni -> Ti](1,6,26,29)**	-0.36515	2.913
	[Al -> Ni](14,17,38,41)** + [Al -> Ti](13,18,37,42)** + [Ni -> Al](2,5,26,29)**	-0.29494	2.919
	[Al -> Ni](13,18,37,42)** + [Al -> Ti](14,17,38,41)** + [Ni -> Al](1,2,5,6)**	-0.29401	2.919
	[Al -> Ni](13,18,37,42)** + [Ni -> Ti](25,26,29,30)**	-0.23489	2.925
	[Al -> Ni](17,18,41,42)** + [Al -> Ti](13,14,37,38)** + [Ni -> Al](5,6,29,30)**	-0.23396	2.925
	[Al ->Ti](13,16,17,20,21,24,37,40,41,44,45,48,61,65,69) + [Ni -> Ti](27,31,35) + [Al -> Ni](64,68,72)+ Ni(2,6,10,50,51,54,55,58,59) <-> Al(14,18,22,38,42,46,62,66,70)	-0.20455	2.935
25.92	[Al -> Ti](13,15,18,21,23,38,41,43,46,61,63,66,69,71)*	-0.50165	2.918
	[Al -> Ti](13,14,17,18,38)*	-0.49371	2.919
31.25	[Al -> Ti](13,18,37,38,41)**	-0.48602	2.930
	[Al -> Ti](13,14,17,18,38)**	-0.44858	2.934

x_{Ti}	Configuration	ΔH (eV/atom)	a (A)
37.50	[Al -> Ti](14,17,37,38,41,42)**	-0.42697	2.947
	[Al -> Ti](14,17,18,37,38,41)**	-0.42467	2.948
	[Al -> Ti](17,18,37,38,41,42)**	-0.41253	2.949
43.75	[Al -> Ti](14,17,18,37,38,41,42)**	-0.38544	2.963
50.00	[Al -> Ti](13,14,17,18,37,38,41,42)**	-0.35202	2.976

REPORT DOCUMENTATION PAGE

1. AGENCY USE ONLY *(Leave blank)*	2. REPORT DATE January 1999	3. REPORT TYPE AND DATES COVERED Technical Memorandum

4. TITLE AND SUBTITLE

BFS Simulation and Experimental Analysis of the Effect of Ti Additions on the Structure of NiAl

6. AUTHOR(S)

Guillermo Bozzolo, Ronald D. Noebe, John Ferrante, Anita Garg, Frank S. Honecy, and Carlos Amador

5. FUNDING NUMBERS

WU–523–22–13–00

7. PERFORMING ORGANIZATION NAME(S) AND ADDRESS(ES)

National Aeronautics and Space Administration
Lewis Research Center
Cleveland, Ohio 44135–3191

8. PERFORMING ORGANIZATION REPORT NUMBER

E–11478

9. SPONSORING/MONITORING AGENCY NAME(S) AND ADDRESS(ES)

National Aeronautics and Space Administration
Washington, DC 20546–0001

10. SPONSORING/MONITORING AGENCY REPORT NUMBER

NASA TM—1999-208892

11. SUPPLEMENTARY NOTES

12a. DISTRIBUTION/AVAILABILITY STATEMENT

Unclassified - Unlimited
Subject Category: 26   Distribution: Nonstandard

This publication is available from the NASA Center for AeroSpace Information, (301) 621–0390.

12b. DISTRIBUTION CODE

13. ABSTRACT *(Maximum 200 words)*

The Bozzolo-Ferrante-Smith (BFS) method for alloy energetics is applied to the study of ternary additions to NiAl. A description of the method and its application to alloy design is given. Two different approaches are used in the analysis of the effect of Ti additions to NiAl. First, a thorough analytical study is performed, where the energy of formation, lattice parameter and bulk modulus are calculated for a large number of possible atomic distributions of Ni, Al and Ti. Substitutional site preference schemes and formation of precipitates are thus predicted and analyzed. The second approach used consists of the determination of temperature effects on the final results, as obtained by performing a number of large scale numerical simulations using the Monte Carlo-Metropolis procedure and BFS for the calculation of the energy at every step in the simulation. The results indicate a sharp preference of Ti for Al sites in Ni-rich NiAl alloys and the formation of ternary Heusler precipitates beyond the predicted solubility limit of 5 at. % Ti. Experimental analysis of three Ni-Al-Ti alloys confirms the theoretical predictions.

14. SUBJECT TERMS

Alloys; Intermetallics; BFS method; Simulations

15. NUMBER OF PAGES
70

16. PRICE CODE
A04

17. SECURITY CLASSIFICATION OF REPORT Unclassified	18. SECURITY CLASSIFICATION OF THIS PAGE Unclassified	19. SECURITY CLASSIFICATION OF ABSTRACT Unclassified	20. LIMITATION OF ABSTRACT